Journal Pre-proof

A facile microwave assisted synthesis and structure elucidation of (3R)-3-alkyl-4,1-benzoxazepine-2,5-diones by crystallographic, spectroscopic and DFT studies

Abdul Rauf Raza, Bushra Nisar, Muhammad Khalid, Humaira Yasmeen Gondal, Muhammad Usman Khan, Sara Figueirêdo de Alcântara Morais, Muhammad Nawaz Tahir, Ataualpa Albert Carmo Braga

PII: S1386-1425(19)31394-0

DOI: https://doi.org/10.1016/j.saa.2019.117995

Reference: SAA 117995

To appear in: *Spectrochimica Acta Part A: Molecular and Biomolecular Spectroscopy*

Received date: 4 September 2019

Revised date: 21 December 2019

Accepted date: 25 December 2019

Please cite this article as: A.R. Raza, B. Nisar, M. Khalid, et al., A facile microwave assisted synthesis and structure elucidation of (3R)-3-alkyl-4,1-benzoxazepine-2,5-diones by crystallographic, spectroscopic and DFT studies, *Spectrochimica Acta Part A: Molecular and Biomolecular Spectroscopy*(2018), https://doi.org/10.1016/j.saa.2019.117995

A Facile microwave assisted synthesis and structure elucidation of (3*R*)-3-alkyl-4,1-benzoxazepine-2,5-diones by crystallographic, spectroscopic and DFT studies

Abdul Rauf Raza,[1]* Bushra Nisar,[2] Muhammad Khalid,[3]* Humaira Yasmeen Gondal,[1] Muhammad Usman Khan,[4] Sara Figueirêdo de Alcântara Morais,[5] Muhammad Nawaz Tahir,[6] Ataualpa Albert Carmo Braga,[5]

[1]*Ibn-e-Sina Block, Department of Chemistry, University of Sargodha, Sargodha-40100, Pakistan*
[2]*Department of Chemistry, The University of Lahore, Sargodha Campus, Sargodha-40100, Pakistan*
[3]*Department of Chemistry, Khwaja Fareed University of Engineering & Information Technology, Rahim Yar Khan-64200, Pakistan*
[4]*Department of Applied Chemistry, Government College University, Faisalabad,38000, Pakistan*
[5]*Departamento de Química, Fundamental, Instituto de Química, Universidade de São Paulo, Avenida Professor LineuPrestes, 748, São Paulo 05508-000, Brazil*
[6]*Ibn-ul-Hathim Block, Department of Physics, University of Sargodha, Sargodha-40100, Pakistan*

Corresponding author[1*] E-mail address: rauf.raza@uos.edu.pk
Corresponding author[3*] E-mail address: Khalid@iq.usp.br ; muhammad.khalid@kfueit.edu.pk

Abstract

The use of microwave (MW) irradiation in organic synthesis has become increasingly popular within the pharmaceutical and academic arenas because it is a new enabling technology for drug discovery and development. It is a rapid way of synthesis, which involves faster reaction rates and high selectivity to conventional heating method of syntheses. The MW-assisted 7-exo-*tet* cyclization of *N*-acylanthranilic acids afforded (3*R*)-3-alkyl-4,1-benzoxazepines-2,5-diones in very short duration (20 min) with extraordinary high yields in comparison to conventional heating mode of synthesis. The method development, comparative yields of MW-assisted and thermal method of syntheses, crystallographic, spectroscopic and density functional theory (DFT) studies are reported herein. Four novel compounds with chemical formulas $C_{10}H_9BrClNO_3$ **5m**, $C_{19}H_{19}NO_3$ **6e**, $C_{13}H_{14}ClNO_3$ **6h** and $C_{12}H_{11}Br_2NO_3$ **6h** were synthesized, validated by ^{1}H-NMR, ^{13}C-NMR, FT-IR, UV-Vis, EIMS spectroscopic techniques and confirmed by using single crystal X-ray diffraction (SC-XRD) study. The DFT and TDDFT calculations at B3LYP/6-311+G(d,p) level of theory were performed for comparative analysis of

spectroscopic data, optimized geometries, frontier molecular orbitals (FMOs), natural bond orbital (NBO) analysis and nonlinear optical (NLO) properties of **5m**, **6e**, **6h** and **6o**. Overall, experimental findings were supported nicely by corresponding DFT computed results. The NBO analysis confirmed that the presence of non-covalent interactions, hydrogen bonding and hyper-conjugative interactions are pivotal cause for the existence of **5m**, **6e**, **6h** and **6o** in the solid-state. NLO analysis showed that **5m**, **6e**, **6h** and **6o** have significant NLO properties as compared to prototype standard compound which disclosed their potential for technology related applications.

Keywords: (3*R*)-3-alkyl-4,1-benzoxazepine-2,5-diones; Microwave irradiation; *N*-acylanthranilic acids; Chiral pool approach; Spectroscopic data; DFT

Introduction

The microwave assisted synthesis offers high reaction rates in shorter time in comparison to conventional heating. The microwave irradiation (MWI) comprises a reduced amount of heating in less time; whereas, greater time and high temperature is required in conventional heating method. For attaining high temperature in conventional heating system an oil bath is used which transfer heat in the system in extended time. The MW passes through the sample and transfer heat to the substrate directly (involving transitions in rotational energy levels) instead of heating whole reaction vessel, thus speeding up a chemical reaction to obtain required results in shorter time interval. The MW speeds up a chemical reaction by transferring heat to the substrate directly (involving transitions in rotational energy levels)rather than heating entire reaction pot in order to obtain desired results in less time thus offering high reaction rates with low utilization of energy. In comparison to conventional heating reaction, MW assisted synthesis offers high reaction rates with energy-conservation while main drawback of conventional heating is the utilization of high heat energy [1, 2]. The benzoxazepines, a flexible heterocycle, offers a wide range of biological activities [3-6]. Due to diversity in activities benzoxazepines attained admirable importance in medicinal chemistry and drug industry; therefore, their synthesis have been of great interest. Mostly reported syntheses, involves conventional heating methods to yield racemic 4,1-benzoxazpine. No MW studies has been reported for the synthesis of 4,1-benzoxazepines.

The synthesis of 1,4-benzoxazepine-3,5-dione reported in literature involves the condensation of 2-bromoethyl-4-oxo-1,3-benzoxaziniumperchlorate with PhCHO followed by treatment with NaOEt solution and intramolecular cyclization [7]. In another report, condensation of the 2-aminophenol with substituted malonyl dichloride afforded 1,5-benzoxazepine-2,4-diones [8]. Single step synthesis of 4,1-benzoxazepine have also been reported by the reaction of *N*-tosyl-1,3-amino- alcohols with bromoethylsulfonium salts followed by intramolecular cyclization [9].

The asymmetric synthesis is gaining popularity in pharmaceutical industry because medicines used nowadays are racemic modifications of two or more enantiomers. Both enantiomers may have different activities and side effects of medicines may be associated with vestigial isomer [10]. To avoid such side-effects asymmetric synthesis (synthesis leading towards pure enantiomer) is the desperate need. High cost of enantiopure / chiral drugs makes them unaffordable/ inaccessible for a community. This factor may be eliminated using inexpensive commercially available starting materials; especially natural products. To synthesize a pure enantiomer, chiral pool methodology (or chiron approach) is an economic method. Our current work not only involved MW assisted synthesis but also involves asymmetric synthesis adopting chiral pool strategy. Our group have reported asymmetric synthesis of (3*R*)-4,1-benzoxazepine-2,5-diones by conventional heating method (3 h heating at 80 °C) in high *ee* [11, 12]. Similar result can be obtained in excellent yield to afford (3*R*)-3-alkyl-4,1-benzoxazepine-2,5-diones *via* MW assisted synthesis (20 min at 100°C).

Herein, we report the synthesis of four novel (3*R*)-3-alkyl-4,1-benzoxazepine-2,5-diones namely; (2′*S*)-2-(2′-chloropropanamido)-5-bromobenzoic acid (**5m**), (3*R*)-3-*iso*-butyl-4,1-benzoxa-zepines-3,5-dione (**6e**), (3*R*)-7-chloro-9-methyl-3-iso-propyl-4,1-benzoxazepines-3,5-dione (**6h**) and (3*R*)-7,9-dibromo-3-*iso*-propyl-4,1-benzoxazepines-3,5-dione (**6o**). The synthesized compounds (**5m**, **6e**, **6h** and **6o**) are validated by ^{1}H-NMR, ^{13}C-NMR, FT-IR, UV-Vis spectroscopic, EIMS spectrometric techniques and finally confirmed by using single crystal X-ray diffraction (SC-XRD) study. Furthermore, utilizing our synthetic as well as computational study background [13-22], we have performed the computational calculations with density functional theory (DFT) to countercheck the spectroscopic and structural characteristics of **5m**, **6e**, **6h** and **6o**. The DFT based computations are performed to estimate frontier molecular orbital (FMO), natural bond orbital (NBO), global reactivity parameters and NLO properties with

respect to **5m**, **6e**, **6h** and **6o**. The ultimate goal of this study involves a precise and thorough account of experimental and theoretical data for clear understanding of structural and spectroscopic aspects of investigated compounds (**5m**, **6e**, **6h** and **6o**).

Materials and methods

All chemicals and reagents of analytical grade were purchased from Merck, Sigma-Aldrich, or Fluka. The pre-coated silica gel (0.25 mm thick layer over Al sheet, Merck) TLC was used to monitor the reaction. The IR and UV/Vis spectra were recorded on Shimadzu (Prestige 21) FT-IR spectrometer as KBr discs and Thermo Spectronic (UV-1700) spectrophotometer in $CHCl_3$/MeOH. The ^{1}H-NMR and ^{13}C-NMR were recorded in $CDCl_3$ on a Bruker AVANCE DPX300/500 (300 or 500 MHz) spectrometer using Me_4Si as internal standard. The EIMS was recorded at 70 *eV* on Fisons Instrument VG Autospec Mass Spectrometer available at HEJ Research Institute of Chemistry (HEJRIC), University of Karachi, Karachi. The single crystal X-Ray data were recorded on Bruker Kappa APEX 11 CCD diffractometer at Department of Physics, University of Sargodha (Pakistan).

Computational procedure

The overall quantum chemical calculations for investigated compounds (**5m**, **6e**, **6h** and **6o**) were accomplished with the help of DFT [23-25] employing Gaussian 09 program package [26]. The XRD driven crystal structures were used for elucidating the initial geometry of **5m**, **6e**, **6h** and **6o**. Complete geometrical optimization was done without symmetry restrictions by applying B3LYP level of DFT and 6-311+G(d,p) basis set combination. The frequency analysis based on DFT/B3LYP/6-311+G(d,p) level of theory was used for confirmation of stability associated with the optimized geometries. The absence of negative eigen values among all calculated frequencies reflected that optimized geometries of **5m**, **6e**, **6h** and **6o** correspond to true minimum at potential energy surfaces. The FMO and NLO analysis was conducted at B3LYP level of DFT and 6-311+G(d,p) basis set conjunction. The NBO analysis was carried out at B3LYP/6-311+G(d,p) level of theory using NBO 3.1 program package [27]. The UV-Vis analysis was performed employing time dependent density functional theory (TDDFT) calculations at B3LYP/6-311+G(d,p) level of theory for estimation of photophysical characteristics of **5m**, **6e**,

6h and **6o**. The input files were organized with the help of Gaussview 5.0 [28]. The Gaussview 5.0, Avogadro [29] and Chemcraft [30] programs were employed for interpreting output files.

Experimental

*Synthesis of (2S)-2-chlorocarboxylic acids (**2a-d**)*

The (2*S*)-2-chlorocarboxylic acids (**2a-d**) were prepared from commercially available inexpensive natural (2*S*)-aminoacids**1a-d** (alanine, phenylalanine, valine and leucine) by following Koppenhoefer's procedure (involving diazotization sequence) [11, 31].

*Synthesis of (2S)-2-chlorocarboxylic acid chlorides (**3a-d**)*

The (2*S*)-2-chlorocarboxylic acid chlorides **3a-d** were prepared by heating (2*S*)-2-chlorocarboxylic acids **2a-d** (3.7 mmol, 1 eq) in $SOCl_2$ (4.1 mmol, 1.1 eq) with two drops of DMF at 80 ºC for 1 h. The reaction demands anhydrous conditions for better results. The resulting (2*S*)-2-chlorocarboxylic acid chlorides (**3a-d**) were used as such without any purification.

*Synthesis of N-acyl anthranilic acids (**5a-p**)*

The (2*S*)-2-chlorocarboxylic acid chloride **3a-d** (0.51 mmol, 1.1 eq) was added to a flask containing anthranilic acid **4** (0.46 mmol, 1 eq) in dry DMF (10 mL) and Et_3N (3.7 mmol, 4 eq). The addition was completed below 0 ºC using ice bath and the resulting solution was stirred overnight at room temperature. The chilled H_2O was added, partitioned with EtOAc (3×15 mL), combined organic layer was separated, dried over anhydrous Na_2SO_4, filtered and concentrated under reduced pressure to afford brown oil, which was column chromatographed over silica gel to afford *N*-acyl anthranilic acids **5a-p** as colourless crystalline solid upon elusion with 1-5% EtOAc in *n*-hexane.

*(2'S)-N-acyl anthranilic acids **5a-j*** [11]

*(2'S)-2-(2'-Chloro-4'-methylpentanamido)-4-chlorobenzoic acid **5k***: R_f: 0.25 (EtOAc/*n*-hexane 3:7); mp: 126 ºC; ύ (cm^{-1}): 1678 (O<u>C=O</u>), 1593 (N<u>C=O</u>), 687 (C–Cl); λ_{max}(log ϵ): 307 nm (3.4792 $L.cm^{-1}.M^{-1}$); δ_H(300 MHz, $CDCl_3$) in ppm: 0.96, 0.98 (3H each, d, *J* = 6.6 Hz, $H^{5'}$& CH_3 at $C^{4'}$), 1.85–1.98 (3H, m, $H^{3'}$& $H^{4'}$), 4.52 (1H, dd, *J* = 9.6, 4.8 Hz, $H^{2'}$), 7.18 (1H, dd, *J* = 8.4, 1.8

Hz, H^5), 8.07 (1H, d, *J* = 8.4, H^6), 8.69 (1H, d, *J* = 1.8. Hz, H^3); δ_C (75 MHz, $CDCl_3$) in ppm: 21.5, 23.0 (q, both $C^{5'}$& CH_3 at $C^{4'}$), 26.5 (d, $C^{4'}$), 45.4 (t, $C^{3'}$), 60.4 (d, $C^{2'}$), 116.4 (s, C^1), 120.9 (d, C^5), 124.5 (d, C^3), 134.0 (d, C^6), 141.1 & 142.8 (s, C^2& C^4), 170.3 and 170.4 (s, both C=O); m/z in amu (% abundance): 307, 305, 303 (1:6:9) $[M]^{+\cdot}$, 251, 249, 247 (1, 6, 9) $[M - C_4H_8]^{+\cdot}$, 182, 180 (1:3) $[M - {}^{\cdot}C_5H_{10}Cl - H_2O]^{+\cdot}$, 172, 170 (1:3) $[M - {}^{\cdot}C_5H_{10}Cl - CO]^{+\cdot}$, 154, 152 (1:3) $[M - H_2O - CO - {}^{\cdot}C_5H_{10}Cl]^{+\cdot}$.

(2'S)-2-(2'-chloro-4'-methylpentanamido)-5-bromobenzoic acid ***5n***: R_f: 0.27 (EtOAc/*n*-hexane 3:7); mp: 117 ºC; ύ (cm^{-1}): 3259 (O–H bs), 3044 (N–H), 1685 (OC=O), 1531 (NC=O), 713 (C–Cl), 559 (C–Br); λ_{max}(log ϵ): 317 nm (3.4789 $L.cm^{-1}.M^{-1}$); δ_H(500 MHz, $CDCl_3$) in ppm: 0.96, 0.98 (3H each, d, *J* = 6.5 Hz, $H^{5'}$& CH_3 at $C^{4'}$), 1.84–1.97 (3H, m, $H^{3'}$& $H^{4'}$), 4.51 (1H, dd, *J* = 8.4, 6.9 Hz, $H^{2'}$), 7.69 (1H, d, *J* = 9.0, 2.5 Hz, H^4), 8.17 (1H, dd, *J* = 2.5 Hz, H^6), 8.53 (1H, d, *J* = 9.0 Hz, H^3); δ_C(125 MHz, $CDCl_3$) in ppm: 21.6, 23.1 (q, both $C^{5'}$& CH_3 at $C^{4'}$), 25.5 (d, $C^{4'}$), 45.5 (t, $C^{3'}$), 60.5 (d, $C^{2'}$), 116.7 (s, C^1), 120.3 (s, C^5), 123.2 (d, C^3), 135.7 (d, C^4), 137.8 (d, C^6), 140.9 (s, C^2), 169.8 and 170.3 (s, both C=O); m/z in amu (% abundance): 351, 349, 347 (1:9:6) $[M]^{+\cdot}$, 305, 303, 301 (1:9:6) $[M - H_2O - CO]^{+\cdot}$, 244, 242 (1:1) $[M - {}^{\cdot}C_5H_{10}Cl]^{+\cdot}$, 295,293,291 (1:9:6) $[M - C_4H_8]^{+\cdot}$, 216, 214 (1:1) $[M - {}^{\cdot}C_5H_{10}Cl - CO]^{+\cdot}$.

(2'S)-2-(2'-chloro-4'-methylpentanamido)-3,5-dibromobenzoic acid ***5p***: R_f: 0.3 (EtOAc/ *n*-hexane 3:7); ύ (cm^{-1}): 1689 (OC=O), 1573 (NC=O), 719 (C–Cl); λ_{max}(log ϵ): 301 nm (3.4065 $L.cm^{-1}.M^{-1}$); δ_H(300 MHz, $CDCl_3$) in ppm: 0.95, 0.99 (3H each, d, *J* = 6.3 Hz, $H^{5'}$& CH_3 at $C^{4'}$), 1.84–1.90 (3H, m, $H^{3'}$& $H^{4'}$), 4.34 (1H, dd, *J* = 9.0, 3.0 Hz, $H^{2'}$), 8.03 (bs, N–H), 8.20 (1H, d, *J* = 1.3 Hz, H^4), 8.38 (1H, d, *J* = 1.3 Hz, H^6); δ_C(75 MHz, $CDCl_3$) in ppm: 21.3, 22.6 (q, both $C^{5'}$& CH_3 at $C^{4'}$), 25.2 (d, $C^{4'}$), 43.4 (t, $C^{3'}$), 55.0 (d, $C^{2'}$), 121.0 (s, C^1), 129.5, 130.0 (s, C^3& C^5), 136.1 (d, C^4), 141.0 (d, C^6), 147.3 (s, C^2), 168.8 and 170.3 (s, both C=O).

Synthesis of 4,1-benzoxazepines ***6a-p***

A mixture of *N*-acyl anthranilic acid **5** (1 mmol, 1 eq) and anhydrous K_2CO_3 (1.5 mmol, 1.5 eq) in DMF (1 mL) was heated under microwave radiations at 100 °C for 20 min. The chilled H_2O was added in excess. The reaction mixture was neutralized with dilute HCl (5 mL) and extracted with EtOAc (2×15 mL). The combined organic extract was dried over anhydrous Na_2SO_4, filtered and concentrated under reduced pressure to afford the crude product. It was purified by

either column chromatography over silica gel or crystallization from EtOAc / *n*-hexane to yield 4,1-benzoxazepines (**6a-p**) in excellent yield (74-100%).

(3R)-3-Alkyl-4,1-benzoxazepine-2,5-diones ***6a-j*** [11]

(3R)-7-Bromo-3-iso-butyl-4,1-benzoxazepines-3,5-dione ***6n***: R_f: 0.70 (EtOAc/*n*-hexane 3:7); mp: 183.3 ºC; ύ (cm^{-1}):1734 (OC=O), 1674 (NC=O), 547.78 (C–Br); λ_{max} (log ϵ) 256.0 nm (3.5956 $L.cm^{-1}.M^{-1}$); δ_H (500 MHz, $CDCl_3$) in ppm: 0.99, 1.02 (3H each, d, *J* = 6.3 Hz, $H^{3'}$ and CH_3 at $C^{2'}$), 1.66 (1H, m, $H^{2'}$), 1.97 (1H, ddd, *J* = -13.4, 6.2, 1.5 Hz, $H^{1'\alpha}$), 2.17 (1H, ddd, *J* = -13.1, 6.1, 1.8 Hz, $H^{1'\beta}$), 4.47 (1H, m, H^3), 7.70 (1H, dd, *J* = 9.0, 2.5 Hz, H^8), 8.04 (1H, s, N–H), 8.28 (1H, d, *J* = 2.5 Hz, H^6), 8.66 (1H, d, *J* = 9.0 Hz, H^9); δ_C (125 MHz, $CDCl_3$) in ppm: 21.3, 25.2 (q, both $C^{3'}$& CH_3 at $C^{2'}$), 28.0 (d, $C^{2'}$), 46.1 (t, $C^{1'}$), 59.9 (d, C^3), 115.9 (s, C^{5a}), 117.2 (s, C^7), 122.1 (d, C^8), 134.3 (d, C^9), 137.8 (s, C^{9a}), 140.0 (d, C^6), 168.9 and 170.4 (s, C^2& C^5).

(3R)-7,9-Dibromo-3-iso-propyl-4,1-benzoxazepine-2,5-dione ***6o****:* R_f: 0.75 (EtOAc /*n*-hexane 3:7); mp: 179 ºC; ύ (cm^{-1}): 1708 (OC=O), 1579 (NC=O), 549 (C–Br); λ_{max} (log ϵ): 249.0 nm (3.4643 $L.cm^{-1}.M^{-1}$); δ_H (500 MHz, $CDCl_3$) in ppm: 0.91, 0.99 (3H each, d, *J* = 6.9 Hz, both CH_3 showing extended diastereotopy), 2.05 (2H, m, $H^{1'}$), 4.51 (1H, m, H^3), 8.01 (1H, bs, N–H), 8.11 (1H, d, *J* = 2.4 Hz, H^6), 8.30 (1H, d, *J* = 2.5 Hz, H^8); δ_C (125 MHz, $CDCl_3$) in ppm: 22.0, 24.9 (q, both CH_3), 29.7 (d, $C^{2'}$), 58.5 (d, C^3), 116.4 (s, C^{5a}), 127.8 (d, C^8), 131.3 (s, C^7), 133.0 (s, C^9), 137.7 (s, C^{9a}), 139.4 (d, C^6), 169.5 and 170.8 (s, C^2& C^5).

(3R)-7,9-Dibromo-3-iso-butyl-4,1-benzoxazepine-2,5-dione ***6p****:* R_f: 0.66 (EtOAc /*n*-hexane 3:7); mp: 176.4 ºC; ύ (cm^{-1}): 1711 (OC=O), 1632 (NC=O), 551 (C–Br); λ_{max} (log ϵ): 234.0 nm (3.2569 $L.cm^{-1}.M^{-1}$); δ_H (500 MHz, $CDCl_3$) in ppm: 0.89, 1.00 (3H each, d, *J* = 6.9 Hz, $H^{3'}$ and CH_3 at $C^{2'}$), 1.57 (1H, m, $H^{2'}$), 2.08 (2H, m, $H^{1'}$), 4.54 (1H, m, H^3), 7.99 (1H, bs, N–H), 8.07 (1H, d, *J* = 2.6 Hz, H^6), 8.26 (1H, d, *J* = 2.6 Hz, H^8); δ_C (125 MHz, $CDCl_3$) in ppm: 22.5, 24.4 (q, both $C^{3'}$& CH_3 at $C^{2'}$), 30.0 (d, $C^{2'}$), 44.1 (t, $C^{1'}$), 57.7 (d, C^3), 116.1 (s, C^{5a}), 129.1 (d, C^8), 130.9 (s, C^7), 133.3 (s, C^9), 138.2 (s, C^{9a}), 139.0 (d, C^6), 169.9 and 171.1 (s, C^2& C^5).

Results and discussion

Keeping the importance of chiron approach and MW assisted organic synthesis in view, the present work is concerned with MW assisted asymmetric (Chiron based) synthesis of 4,1-benzoxazepines. For this purpose (–)-(*S*)-2-chlorocarboxylic acids **2a-d** were prepared in high *ee* (95%–98%) *via* diazotization of naturally occurring (+)-(*S*)-amino acids **1a-d** (alanine, phenylalanine, valine and leucine) [31]. These (–)-(*S*)-2-chlorocarboxylic acids **2a-d** were converted to (*S*)-2-chlorocarboxylic acid chlorides **3a-d** and coupled with substituted anthranilic acids **4** to afford (2′*S*)-*N*-acylanthranilic acids **5a-p**. Conventionally, the base mediated 7-exo *tet* cyclization of (2′*S*)-*N*-acylanthranilic acids **5a-p** takes longer duration (3 h) to afford (3*R*)-3-alkyl-4,1-benzoxazepine-2,5-diones **6a-p**. Whereas, MW assisted synthesis of (2′*S*)-*N*-acylanthranilic acids **5a-p** affords (3*R*)-3-alkyl-4,1-benzoxazepine-2,5-diones **6a-p** in shorter interval with excellent yield (Scheme 1, Table 1).

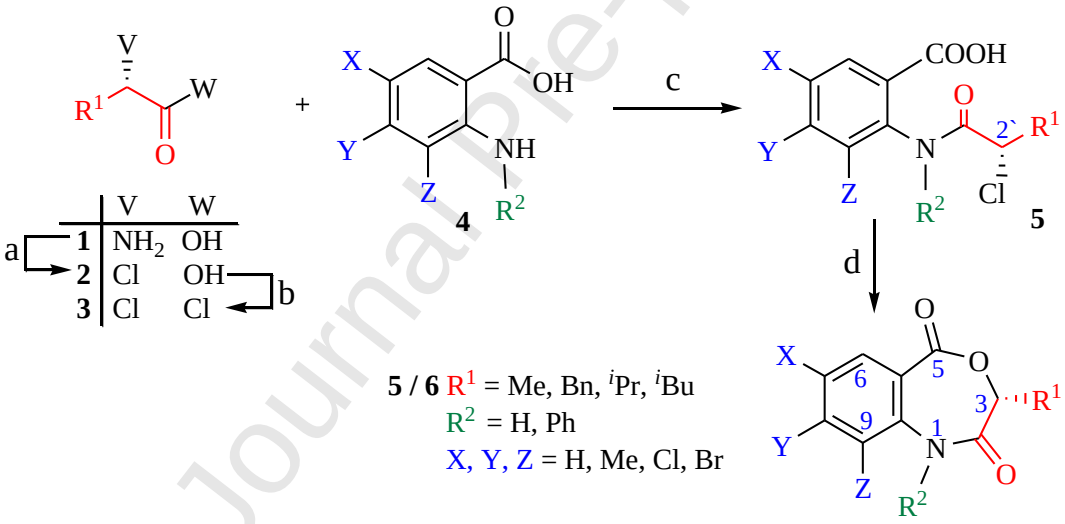

Reagents and condition: **a**) *aq* $NaNO_2$, HCl (10*N*), below –10°C;**b**) $SOCl_2$ (1.1 eq), DMF (1 drop); **c**) drop wise addition of **3** to **4**, DMF, 0 °C; **d**) K_2CO_3, DMF, 100 °C (20 min), MWI.

Scheme 1: Methodology designed for the synthesis of (3*R*)-3-alkyl-4,1-benzoxazepine-2,5-diones **6a-p**.

Table1: Comparison of %yield of 4,1-benzoxazepines obtained *via* conventional heating and MW assisted organic synthesis.

Entry	6	Substituents					% Yield	
		R^1	R^2	X	Y	Z	C*	MW^
1	**a**	Me	H	H	H	H	76	94
2	**b**	^{i}Pr	H	H	H	H	70	90
3	**c**	^{i}Bu	H	H	H	H	71	75
4	**d**	Bn	H	H	H	H	50	80
5	**e**	^{i}Bu	Ph	H	H	H	66	89
6	**f**	^{i}Pr	H	H	H	Me	62	100
7	**g**	^{i}Bu	H	H	H	Me	86	93
8	**h**	^{i}Pr	H	Cl	H	Me	65	97
9	**i**	^{i}Bu	H	Cl	H	Me	62	100
10	**j**	Me	H	H	Cl	H	68	75
11	**k**	^{i}Bu	H	H	Cl	H	59	85
12	**l**	Bn	H	H	Cl	H	63	94
13	**m**	Me	H	Br	H	H	55	82
14	**n**	^{i}Bu	H	Br	H	H	49	89
15	**o**	^{i}Pr	H	Br	H	Br	51	81
16	**p**	^{i}Bu	H	Br	H	Br	33	75

*Conventional heating; ^MW irradiation

In current study, the main focus was to probe the effect of temperature (°C) and time (min) on MW assisted heating on the final cyclization step in contrast to conventional heating method. So, the reaction conditions were primarily inspected by changing temperature followed by time. For optimization of cyclization reaction under MW exposure, different reaction conditions were employed including variation in temperature (50-150 °C) and time (5-30 min) (Table 2). It was observed that at 50 °C no product formation was observed at variable time duration (5-30 min). The best results were obtained at 100 °C for 20 min duration exposure to MW irradiations. Upon increasing reaction duration at 100 °C, a number of products start appearing; whereas, at 150 ºC it decomposed to black mass.

Table 2: Optimization of reaction temperature and time duration for **5c**.

Entry	T (°C)§	Time (min)	**6c** (%)	Entry	T (°C)§	Time (min)	**6c** (%)
1	50	5	-	19	80	5	15
2		10	-	20		10	20
3		15	-	21		15	25
4		20	-	22		20	25
5		25	-	23		25	30
6		30	-	24		30	30

7	60	5	*	25	90	5	35
8		10	*	26		10	35
9		15	*	27		15	40
10		20	*	28		20	45
11		25	*	29		25	50
12		30	*	30		30	50
13	70	5	2	31	100	5	60
14		10	6	32		10	65
15		15	8	33		15	70
16		20	10	34		20	75
17		25	10	35		25	^
18		30	15	36		30	^
				37	150	5	Decompose

[§]200 W power lamp; [*]product formed in traces; [^]number of products formed

Based on the initial trails, it is concluded that best reaction time is 20 min and best reaction temperature is 100 °C for maximum conversion of a *N*-acylanthranilic acid **5** to a 4,1-benzoxazepine-2,5-dione **6**. The final cyclized 4,1-benzoxazepines **6a-p** were identified through mass spectrometry coupled with GC. The results of the GC/MS analysis showed the formation of pure benzoxazepine, which were identified by mass spectrometry coupled to GC (Figure 1).

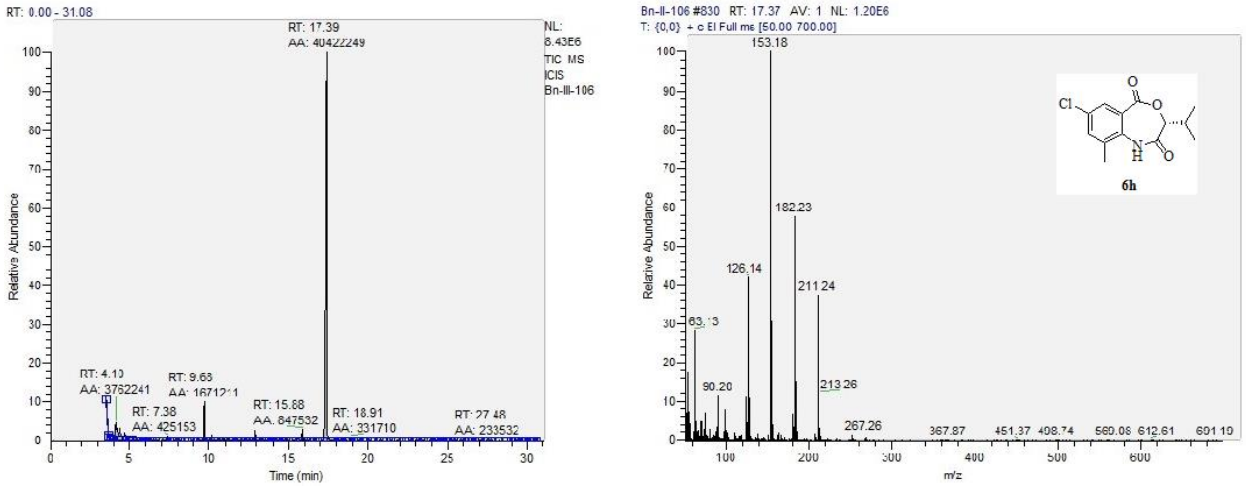

Figure 1. The GC/MS analysis of 4,1-benzoxazepines **6h**. The gas chromatogram (*left*) is ensuring the purity of **6h**. The Electron Impact mass spectrum(*right*) is characterizing the compound, which is showing same fragmentation pattern to already synthesized compounds by conventional heating.

The EIMS of all synthesized 4,1-benzoxazepines **6a-p** by MWI were found in match with already synthesized 4,1-benzoxazepines **6a-o** by conventional heating method. The molecular ions of **6b** and **6c** were observed at 219 and 233 amu respectively, which confirms the formation of 4,1-benzoxazepines under MW exposure. Following fragmentation pattern is suggested for **6b** and **6c**. These molecular ions subsequently fragmentize by logical loss of oxirane ring (following β-keto cleavage or step-wise cleavage) to result a common radical cation A (Figure 2).

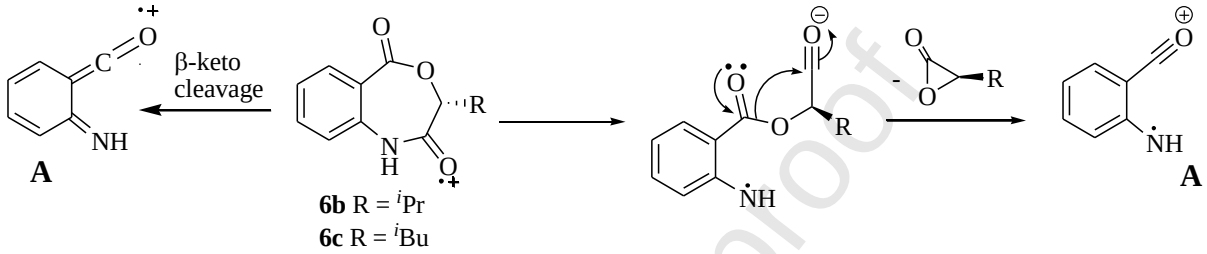

6	$[M]^{+\bullet}$ (%)	A (%)
b	219 (20)	119 (100)
c	233 (40)	119 (32)

Figure 2. The mass fragmentation pattern of a few synthesized 4,1-benzoxazepines (**6b-c**).

Crystallographic Description

The parameters of data collection along with data refinements for crystals of **5m**, **6e**, **6h** and **6o** are presented in following Table 3.

Table 3: Crystallographic data of compounds **5m**, **6e**, **6h** and **6o**.

Crystal data	**5m***	**6e***	**6h***	**6o***
CCDC	1940454	1940456	1940457	1940455
Chemical formula	$C_{10}H_9BrClNO_3$	$C_{19}H_{19}NO_3$	$C_{13}H_{14}ClNO_3$	$C_{12}H_{11}Br_2NO_3$
M_r	306.54	309.35	267.70	377.04
Crystal system, space group	Triclinic, $P\bar{1}$	orthorhombic, *Pbca*	Monoclinic, $P2_1/c$	Triclinic, $P\bar{1}$
Temperature (K)	296	296	296	296
a, *b*, *c* (Å)	4.8491 (6)	10.9472 (15)	8.8100 (7)	5.2145(6)
	10.5133 (14)	9.2516 (11)	21.1270 (16)	9.584 (2)
	12.2128 (17)	33.456 (6)	6.9337 (5)	13.919 (3)
α, β, γ (°)	76.894 (4)	90	90	87.284 (5)
	83.670 (3)	90	97.740 (4)	80.424 (7)
	82.599 (4)	90	90	86.318 (6)
V (Å^3)	599.22 (14)	3388.4 (8)	1286.15(17)	684.0 (2)

Z	2	8	4	2
Density (calculated)	1.699 Mg/m^3	1.213 Mg/m^3	1.383 Mg/m^3	1.831Mg/m^3
F(000)	304	1312	560	368
Radiation type	Mo *K*α			
Wavelength (λ)	0.71073 Å			
μ (mm^{-1})	3.643	0.082	0.296	5.924
Crystal size (mm)	0.38 × 0.26 × 0.22	0.35 × 0.18× 0.16	0.30 × 0.24 × 0.20	0.40 × 0.26 × 0.24
Data Collection				
Diffractometer	Bruker APEXII CCD diffractometer			
Absorption correction	Absorption correction:multi-scan (SADABS; Bruker, 2007)			
No. of measured, independent and observed [*I*> 2s(*I*)] reflections	7179, 2576, 1803	13106, 3151, 1576	11414, 2794, 2011	7797, 2958, 1882
R_{int}	0.030	0.060	0.042	0.040
Theta range for data collection	2.905 to 27°	1.217 to 25.5°	1.928 to 27°	1.332 to 27°
Index ranges	-5≤ h ≤6, -13≤ k ≤ 13, -15≤ l ≤ 15	-8≤ h ≤13, -7≤ k ≤ 11, -37 ≤ l ≤40	-11≤ h ≤11, -26≤ k ≤26, -5 ≤ l ≤8	-6≤ h ≤6, -12≤ k ≤ 12, -17≤ l ≤17
$(\sin\theta/\lambda)_{max}$ (Å^{-1})	0.639	0.606	0.639	0.639
Refinement				
$R[F^2> 2\sigma(F^2)]$, $wR(F^2)$, *S*	0.051, 0.140, 1.04	0.053, 0.142, 1.00	0.053, 0.152, 1.05	0.043, 0.090, 1.01
No. of reflections	2576	3151	2794	2958
No. of parameters	147	210	167	165
H-atom treatment	H-atom parameters constrained	H-atom parameters constrained	H atoms treated by a mixture of independent and constrained refinement	H-atom parameters constrained
$\Delta\rho_{max}$, $\Delta\rho_{min}$ (e Å^{-3})	0.59, -0.54	0.15, -0.19	0.37, -0.25	0.67, -0.63

*The compounds (**5m**, **6e**, **6h** and **6o**) are given SWA7UOS, BN-III-68, BN-III-86 and SWC1UOS code names in CIF files.

Table 4: Hydrogen-bond geometry (Å, º) in **5m**, in **6e**, **6h** and **6o.**

	D—H···*A*	*D*—H	H···*A*	*D*···*A*	*D*—H···*A*
5m	O1—H1···O2^{i}	0.82	1.82	2.643 (3)	177
	N1—H1*A*···O2	0.86	2.00	2.660 (3)	133
	C5—H5···O3^{ii}	0.93	2.44	3.345 (4)	165
6e	C16—H16*A*···O2^{iii}	0.97	2.51	3.463 (3)	166
	C4—H4···O2^{iv}	0.93	2.40	3.271 (3)	157
	C12—H12···O3^{v}	0.93	2.44	3.295 (4)	153
6h	N1—H1*A*···O3^{vi}	0.86	2.06	2.909 (3)	170
6o	N1—H1*A*···O3^{vii}	0.86	2.10	2.933 (4)	164
	N1—H1*A*···Br2	0.86	2.75	3.035 (3)	101

Symmetry codes: (i) –*x*−1, −*y*, −*z*+1; (ii) –*x*+1, −*y*+1, −*z*+1; (iii) –*x*+1/2, *y*+1/2, *z*; (iv) –*x*+3/2, *y*+1/2, *z*; (v) *x*+1/2, *y*, −*z*+1/2; (vi) −*x*, −*y*, −*z*; (vii) − *x*, − *y*, − *z* + 1.

(2'S)-2-(2'-Chloropropanamido)-5-bromobenzoic acid 5m

In **5m** (Figure 3a), the 2-amino-5-bromobenzoic acid moiety A (C1-C7/N1/O1/O2/Br1) and 2-chloropropanoyl part B (C8-C10/O3) are planar with r. m. s. deviation of 0.0300 and 0.0010 Å, respectively. The dihedral angle between A/B is 13.1 (5)°. The Cl1 atom is at a distance of -1.0461 (13) Å from the mean square plane of B or the orientation of Cl1-atom can be evaluated from the torsion angle of N1-C8-C9-Cl1 which is 43.2(7)°. The intramolecular H-bonding of N-H…O and N-H…Cl1 complete S (6) and S (5) loops [32] respectively. The molecules are dimerized through conventional loops $R_2^2(8)$ due to O-H…O bonding [Figure 3b, Table 4]. The dimers are further interlinked due to C-H…O bonds and complete $R_2^2(14)$ loop.

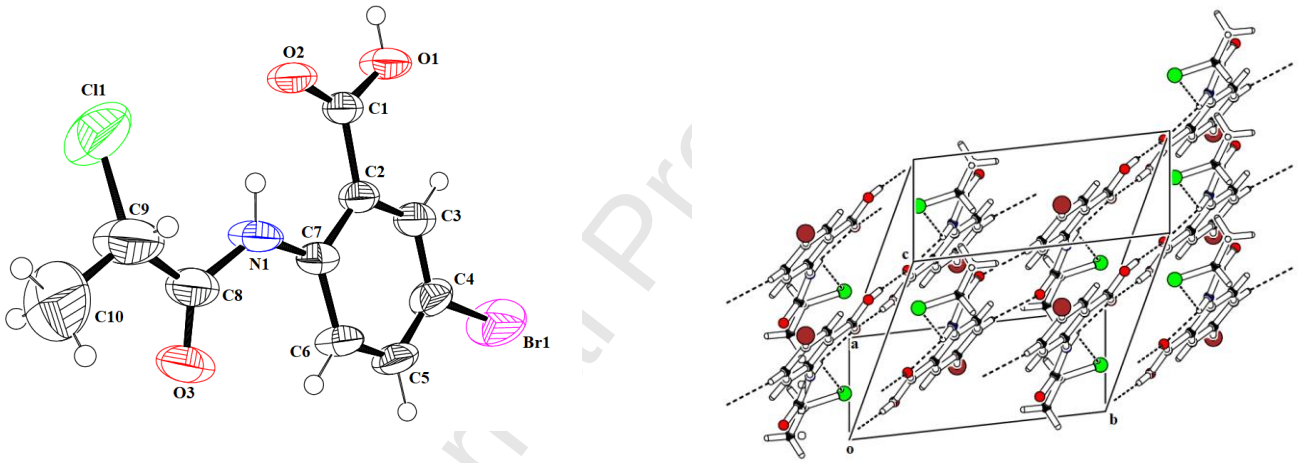

(**a**) The ORTEP presentation (**b**) The H-bonding pattern

Figure 3. (**a**) The ORTEP presentation of **5m** with thermal ellipsoids drawn at 50 % probability level with H-atoms drawn as small circles of arbitrary radii; (**b**) The H-bonding pattern showing the C(6) chain due to N-H…O interaction.

(3R)-3-Iso-butyl-4,1-benzoxazepines-3,5-dione 6e

In **6e** (Figure 4a), the benzene ring A (C2-C7) and the aniline moiety B (C10-C15/N1) are planar with r. m. s. deviations of 0.0026 and 0.0104 Å respectively. The *iso*-butyl moiety is roughly planar with r. m.s. deviation of 0.2044 Å. The dihedral angle between A/B, A/C and B/C is 78.56 (7)°,54.68 (12)° and 81.77 (10)° respectively. The part of carboxyl group D (C1/O1/O2) and the ethylene part E (C8/C9/O3) are of course planar. The dihedral angle between C/D, C/E and D/E is 87.24 (24)°, 30.7 (3)° and 61.8 (3)° respectively. Each molecule is attached through three C-

H····O bonding with three adjacent molecules (Figure 4b, Table 4). There does not exist any appreciable π····π interaction.

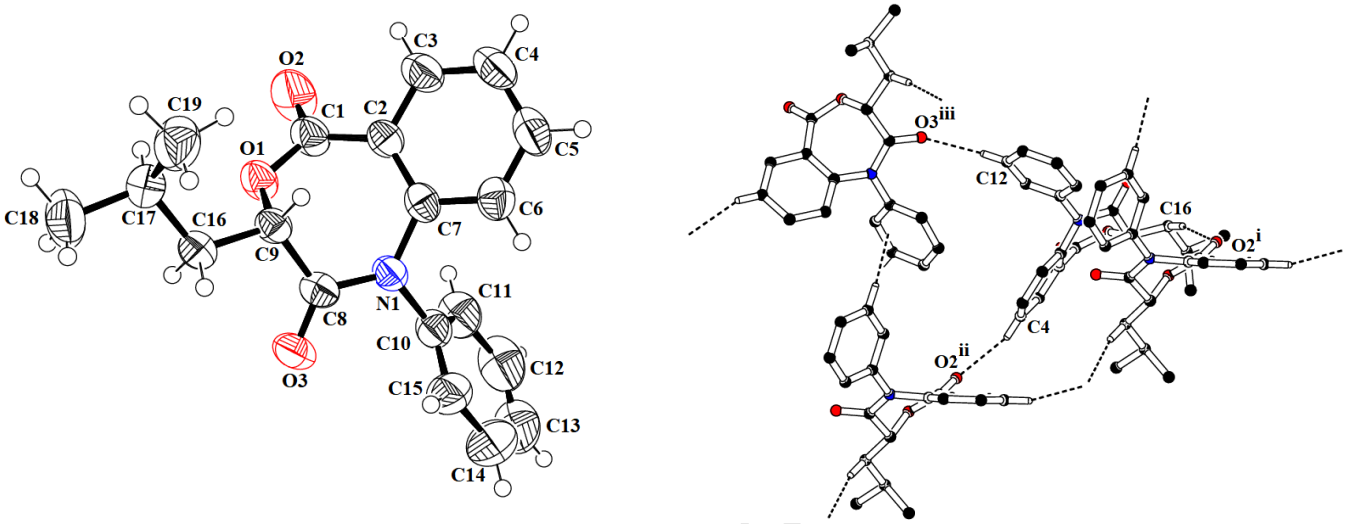

(**a**) The ORTEP presentation (**b**) The H-bonding pattern

Figure 4. (**a**) The ORTEP presentation of **6e** with thermal ellipsoids drawn at 50 % probability level with H-atoms drawn as small circles of arbitrary radii; (**b**) The H-bonding pattern showing that the molecules are linked with three adjacent molecules due to H-bonding.

(3R)-7-Chloro-9-methyl-3-iso-propyl-4,1-benzoxazepines-3,5-dione 6h

In **6h** (Figure 5a), the 4-chloro-2-methylaniline moiety A (C1-C6/C10/N1/Cl1) is planar with r. m. s. deviation of 0.0113 Å. The lactonic part B (C7/O1/O2), the ethanoylpart C (C8/C9/O3) and *iso*-propyl moiety D (C11/C12/C13) are of course planar. The dihedral angles between A/B, A/C, A/D, B/C, B/D and C/D are 38.32 (14)°, 36.95 (25)°, 86.6 (3)°, 65.2 (3)°, 76.2 (4)° and 76.0 (3)° respectively. The molecules are dimerized due to N–H····O boding and complete $R_2^2(8)$ loop (Figure 5b, Table 4).

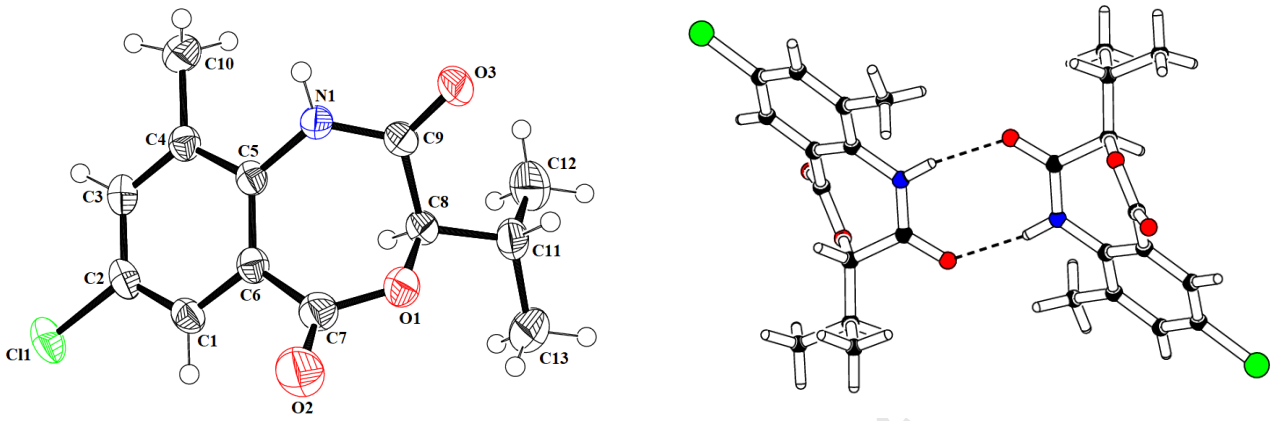

(**a**) The ORTEP presentation (**b**) The H-bonding pattern

Figure 5. (**a**) The ORTEP presentation of **6h** with thermal ellipsoids drawn at 50 % probability level with H-atoms drawn as small circles of arbitrary radii; (**b**) The H-bonding pattern showing the $R_2^2(8)$ loop.

(3R)-7,9-Dibromo-3-iso-propyl-4,1-benzoxazepines-3,5-dione 6o

In **6o** (Figure 6a), the benzene ring A (C1-C6) is planar with r. m. s. deviation of 0.0068 Å. The attached bromine atoms (Br1 and Br2) are at a distance of -0.024 (5) and 0.123 (5) Å from the mean square plane. The seven membered ring is like a boat conformation with basal plane B (N1/C7/O1/C9) having r. m. s. deviation of 0.0096 Å. The apical planes of boat conformation are C (C5/C6/C7/N1) (r. m. s. deviation of 0.0061 Å) and D (C8/C9/O1). The dihedral angle between A/B, B/C and B/D is 28.6 (2)°, 32.7 (2)° and 61.3 (2)° respectively. The molecules are dimerized due to N–H···O bonding with $R_2^2(8)$loop (Figure 6b, Table 4). The deviation of Br2 from the benzene ring is due to N–H···Br bonding with it (as shown in the Figure 6b). The N–H···Br bonding complete S(5) ring.

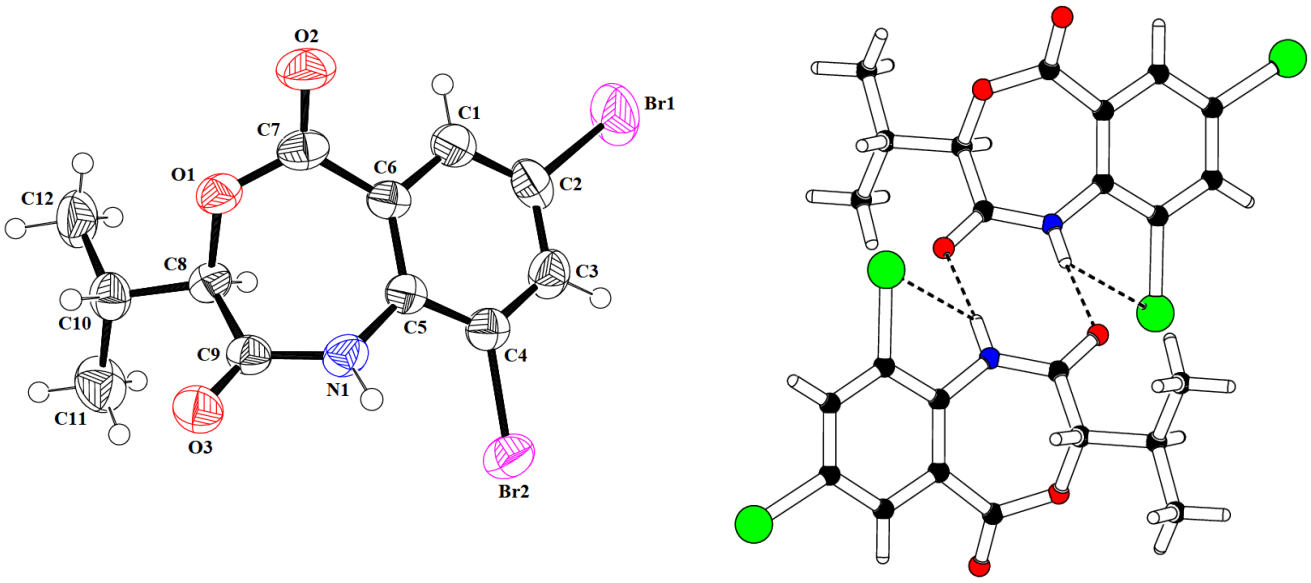

(**a**) The ORTEP presentation (**b**) The H-bonding pattern

Figure 6. (**a**) The ORTEP presentation of **6o** with thermal ellipsoids drawn at 50 % probability level with H-atoms drawn as small circles of arbitrary radii; (**b**) The H-bonding pattern showing that molecules are dimerized.

Computational studies

Geometric structures

The optimized geometric parameters (bond lengths and bond angles) of **5m**, **6e**, **6h** and **6o** have been determined by using B3LYP/6-311+G(d,p) functional. The comparative study is done between DFT calculated and experimentally determined parameters obtained through XRD. Atom numbering scheme as shown in Figures 3a, 4a, 5a and 6a for respective **5m**, **6e**, **6h** and **6o** compounds are used to calculate the DFT and XRD structural parameters and results are collected in Tables S1-S4 (Supplementary Information). A graphical representation of comparison between SC-XRD and DFT based bond lengths and bond angles have been portrayed in Figures S1-S4 (Supplementary information) respectively.

Overall, maximum deviation in bond lengths is observed in the ambient of 0.048 ± 0.005Å, 0.033 ± 0.004Å, 0.035 ± 0.007Å and 0.032 ± 0.013Å in **5m**, **6e**, **6h** and **6o** respectively. In case of bond angles, 8.7° ± 2.6°, 1.3° ± 0.8°, 2.4° ± 1.1° and 1.9° ± 1.1° are the divergence ranges noticed in **5m**, **6e**, **6h** and **6o** respectively. In **5m**, the maximum and minimum deviation in bond length is noticed for C(9)-C(10) and O(2)-C(1) bonds respectively. The bond angles which are deviated utmost and least in **5m** are found to be in Cl(1)-C(9)-C(10) and O(2)-C(1)-C(2) respectively. The bond lengths C(13)-C(14) and O(1)-C(9) are found to be with maximum and minimum deviation in **6e**. The bond angle in **6e** is diverged to large extent in O(1)-C(1)-C(2) and minutely in C(1)-O(1)-C(9), O(1)-C(1)-O(2), O(1)-C(9)-C(16) respectively. The maximum and minimum deviation in bond lengths of **6h** is found to be for N(1)-C(9) and O(3)-C(9), N(1)-C(5) respectively. Similarly, C(7)-O(1)-C(8) and O(3)-C(9)-N(1) are the bonds of **6h** in which maximum and minimum deviations of angles are observed. In case of **6o**, bond length and angle are found be deviated to large extent in N(1)-C(9), C(5)-N(1)-C(9) and to less extent in O(3)-C(9), Br(2)-C(4)-C(3) bonds respectively. The comparative analysis revealed that SC-XRD and DFT based empirically determined values of bond angles and bond lengths coincide nicely with each other. The third digit difference between SC-XRD and DFT functional findings is observed in most of the values. Briefly, some DFT values deviates when comparing with the SC-XRD data and these differences are probably due to intramolecular interactions in the solid state. Despite of these minute differences, the calculated geometrical parameters attained using DFT

and SC-XRD indicate that both structural parameters are in good agreement with each other and can provide a starting point to calculate other properties.

For a fair comparison between the experimental and TD-DFT/DFT study regarding optimization, error was further calculated with the help of the following equations 1-4:

$$\text{Mean Absolute Deviation (MAD)} = \frac{\sum_{t=1}^{n} |EXP - DFT|}{n} \qquad \text{Equation 1}$$

Where n is total number of Bond Length or Bond Angle values considered, t is number of bond length or bond angle value, EXP is the experimental bond length or bond angle value and DFT is the DFT study based bond length or bond angle value. The mean absolute deviation (MAD) is the sum of absolute differences between the experimental value and the DFT study based value divided by the total number of bond length or bond angle values taken.

$$\text{Mean Square Error (MSE)} = \frac{\sum_{t=1}^{n} (EXP - DFT)^2}{n} \qquad \text{Equation 2}$$

Mean square error is commonly used error metric. It penalizes large errors because squaring larger numbers has a greater impact than squaring smaller numbers.

$$\text{Root Mean Square Error (RMSE)} = \sqrt{\frac{\sum_{t=1}^{n} (EXP - DFT)^2}{n}} \qquad \text{Equation 3}$$

The root mean square error (RMSE) is the square root of MSE and is the most commonly used error metric and had been especially considered for the derivatives under study.

$$\text{Mean Absolute Percentage Error (MAPE)} = \frac{\sum_{t=1}^{n} \left|\frac{EXP - DFT}{EXP}\right|}{n} \times 100 \qquad \text{Equation 4}$$

Mean Absolute Percentage Error (MAPE) is the average of absolute errors divided by the experimental values.

As discussed, the error calculations from equations 1-4 are presented in Table S5 (Supplementary information). The RMSE value is considered to be the most commonly used one, so, for the derivatives, the values for RMSE are found good in case of bond lengths and the bond angles. But, in case of bond angles, the values in **5m** showed larger figures due to the C-Cl bonds.

FT-IR analysis

In present study, nature of vibrational modes, harmonic frequencies and intensities of the vibrational bands present in **5m**, **6e**, **6h** and **6o** were examined theoretically at DFT/B3LYP/6-311+G(d,p) level of theory. Utilizing Gaussview animation option, vibrational modes present in **5m**, **6e**, **6h** and **6o** were assigned. The experimental spectrums of **5m**, **6e**, **6h** and **6o** are displayed in Figures S5-S8 (Supplementary information). The calculated FT-IR results along with their detailed assignments and experimental FT-IR results of **5m**, **6e**, **6h** and **6o** are presented in Tables S6-S9 (Supplementary information**)** correspondingly.

C–H stretching vibrations

It is revealed from literature study that vibrational bands in the ambient of 3100-3000 cm^{-1} are observed as a consequence of C-H vibrations of aromatic ring [33]. In present study, the aromatic ring C–H stretching vibrations for **5m**, **6e**, **6h** and **6o** are measured in the ranges of 3243-3093 cm^{-1}, 3205-3168 cm^{-1}, 3217-3192 cm^{-1} and 3219-3217 cm^{-1} respectively (Tables S6-S9). Pure symmetric and asymmetric vibrations in **5m** are observed with stretching frequencies of 3093 cm^{-1}, 3231 cm^{-1}, 3243 cm^{-1} and 3199 cm^{-1} respectively. In **6e**, bands observed with frequencies 3194 cm^{-1}, 3204 cm^{-1}, 3205 cm^{-1} are assigned to pure symmetric vibrations, while pure asymmetric C-H stretching vibrations are observed at 3168 cm^{-1}, 3174 cm^{-1}, 3185 cm^{-1}, 3189 cm^{-1} and 3201 cm^{-1} wavenumbers. Similarly, pure symmetric vibrational bands are calculated with stretching frequencies 3192 cm^{-1}, 3217 cm^{-1} in **6e** and 3217 cm^{-1}, 3219 cm^{-1} in **6h** respectively. The rocking mode of vibrations in **5m**, **6e**, **6h** and **6o** are located with vibrational bands present in the span of 934-1635 cm^{-1}, 633-1352 cm^{-1}, 739-1617 cm^{-1} and 767-1581 cm^{-1} respectively.

C-C stretching vibrations

The stretching frequency associated with C-C bond of ring frame work and derivatives usually appears in the range of 1650-1400 cm^{-1} [34, 35]. In our investigated molecules **5m**, **6e**, **6h** and **6o,** sharp bands in the ranges of 428-1635 cm^{-1}, 418-1639 cm^{-1}, 408-1624 cm^{-1} and 476-1615 cm^{-1} respectively are computed due to C-C stretching vibrational modes (Tables S6-S9). Furthermore, almost similar peaks have been found for both theoretical and experimental findings. The C-C stretching vibrations in **5m** have been observed through DFT at 528, 808,

1309, 1417 and 1483 cm^{-1} which are strongly supported by experimental C-C vibrational wavenumbers located at 534, 807, 1311, 1423 and 1486 cm^{-1} respectively (Table S6).

The DFT calculated data in **6e** showed vibrational bands at 432, 520, 619, 696, 769, 997, 1132, 1253 and 1330 cm^{-1} which show good resemblance with the experimentally observed bands at 428, 518, 616, 693, 771, 993, 1137, 1258 and 1326 cm^{-1} respectively (Table S7). In **6h,** stretching modes of C-C computed at 790, 929, 1024, 1132, 1261, 1298 and 1423 cm^{-1} describe excellent agreement with experimental bands found at 793, 933, 1021, 1131, 1267, 1283 and 1429 cm^{-1} respectively (Table S8). Similar trend is noticed in **6o** molecule with nice harmony among DFT computed bands (695, 904, 1232, 1309, 1417 and 1589 cm^{-1}) and experimental calculated stretching frequencies (698, 923, 1232, 1319, 1412 and 1581 cm^{-1}) respectively (Table S9).

Methyl group vibrations

The skeleton of **5m**, **6e**, **6h** and **6o** contain methyl groups. The characteristics region to recognize the attendance of methyl group C–H stretching vibrations is 3000-2800 cm^{-1} [36]. In **5m**, vibrational bands located at 3042, 3110 cm^{-1} and 3142 cm^{-1} are assigned to the symmetric and asymmetric C–H stretching vibrations of methyl group respectively (Table S6). The peaks for symmetric and asymmetric methyl group vibrations in **6e** are observed at wave-numbers 3012, 3016, 3026, 3041 cm^{-1} and 3052, 3072, 3079, 3082, 3091 cm^{-1} respectively (Table S7). In **6h,** methyl group C–H bands observed at 3014, 3017, 3019, 3021, 3054 cm^{-1} are due to pure symmetric stretching vibrations, while those observed at 3067, 3080, 3089, 3117, 3119, 3121 cm^{-1} are owing to the asymmetric vibrational modes of methyl group (Table S8). Similarly in **6o,** symmetric vibrations of methyl group C–H are found to be with wavenumbers 3019, 3020, 3023 and 3055 cm^{-1}, whereas asymmetric vibrational modes of methyl group C–H are observed with stretching frequencies 3082, 3091, 3121 and 3122 cm^{-1} respectively (Table S9). Furthermore, DFT computed wavenumber at 3072 in **6e** and 3080, 3089 in **6h** exhibit good agreement with experimental calculated stretching frequency values found at 3072 in **6e** and 3086 in **6h** respectively. The rocking mode of vibrations present in methyl group C–H bond of **5m**, **6e**, **6h** and **6o** molecules are located in the ambient of 233-1378 cm^{-1}, 233-1377 cm^{-1}, 211-1369 cm^{-1} and 215-1404 cm^{-1} respectively.

C=O group vibration

According to our findings, the C=O stretching modes are observed with sharp bands at 1764 cm^{-1} in **5m**, at 1756, 1785 cm^{-1} in **6e,** at 1769, 1785 cm^{-1} in **6h** and at 1776, 1788 cm^{-1} in **6o** respectively.

N-H group vibration

Owing to the possibility of overlapping with several other vibrations, the evaluation of N-H bands is usually hard. The stretching vibrations for pure N-H group are found to be at 3443 cm^{-1}, 3587 cm^{-1} and 3554 cm^{-1} in **5m**, **6h** and **6o** respectively.

From the preceding discussion, it is evident that DFT computed results associated well with the corresponding experimental results given in Tables S6-S9 (Supplementary information**)**

Natural bond orbitals (NBO) analysis

NBO investigation was carried out at B3LYP/6-311+G(d,p)level of theory using Gaussian embedded NBO 3.1 program package [27] to examine the charger transfer between filled (donor) Lewis-type bonding NBOs to the vacant (acceptor) non-Lewis anti-bonding NBOs [37, 38], hyper-conjugative interactions (HCI), inter and intra-molecular bonding and presence of hydrogen bonding (HB) in **5m**, **6e**, **6h** and **6o.** The second order stabilization energy $E^{(2)}$ has laid on the line association to the intensity of energy between donor and acceptor. The second order stabilization energy $E^{(2)}$ can be defined by equation 5 [39].

$$E^{(2)} = q_i \frac{(F_{i,j})^2}{\varepsilon_j - \varepsilon_i} \qquad \text{Equation (5)}$$

Where q_i is the donor orbital occupancy, $\varepsilon_j$and ε_i are diagonal elements and F(i,j) is the off-diagonal NBO fock matrix element. The second order perturbation theory analysis display diverse description of HCIs among which representative NBO values are displayed in Table 5.

Table 5: Representative natural bond orbital (NBO) data for **5m**, **6e**, **6h** and **6o**.

Compound	Donor(i)	Type	Acceptor (j)	Type	E(2)[a] [kcal/mol]	E(j)–E(i)[b] [a.u.]	F(i;j)[c] [a.u.]
5m	C2-C7	π	C3-C4	π*	24.20	0.28	0.075
	C3-C4	π	C2-C7	π*	14.92	0.28	0.060
	C5-C6	π	C2-C7	π*	24.08	0.27	0.073
	O1	LP(2)	O2-C1	π*	59.91	0.31	0.125
	O2	LP(1)	O1-C1	σ*	20.53	0.71	0.110
	N1	LP(1)	C2-C7	π*	41.99	0.27	0.098
	C2'-C7'	π	C3'-C4'	π*	24.20	0.28	0.075
	C3'-C4'	π	C2'-C7'	π*	14.92	0.28	0.060
	C5'-C6'	π	C2'-C7'	π*	24.08	0.27	0.073
	O1'	LP(2)	O2'-C1'	π*	59.91	0.31	0.125
	O2'	LP(1)	O1'-C1'	σ*	20.53	0.71	0.110
	N1'	LP(1)	C2'-C7'	π*	41.99	0.27	0.098
	O2	LP(2)	O1'-H1'	σ*	17.64	0.70	0.101
	O2'	LP(2)	O1-H1	σ*	17.64	0.70	0.101
	O2	LP(2)	N1-H1A	σ*	5.16	0.74	0.057
	O2'	LP(1)	N1'-H1A'	σ*	5.24	1.14	0.069
6e	C2-C7	π	C3-C4	π*	19.66	0.30	0.070
	C3-C4	π	C5-C6	π*	21.62	0.28	0.070
	C5-C6	π	C2-C7	π*	21.74	0.28	0.071
	C10-C11	π	C14-C15	π*	20.18	0.29	0.069
	C12-C13	π	C10-C11	π*	21.32	0.28	0.069
	C14-C15	π	C10-C11	π*	21.38	0.28	0.069
	O1	LP(2)	O2-C1	π*	33.61	0.38	0.101
	O2	LP(2)	O1-C1	σ*	32.13	0.62	0.128
	O3	LP(2)	N1-C8	σ*	27.59	0.68	0.124
	N1	LP(1)	O3-C8	π*	53.48	0.28	0.112
	O2	LP(2)	C9-H9	σ*	2.84	0.71	0.042
6h	C1-C2	π	C3-C4	π*	20.29	0.31	0.070
	C3-C4	π	C5-C6	π*	21.13	0.28	0.069
	C5-C6	π	C1-C2	π*	21.15	0.29	0.070
	O1	LP(2)	O1-C7	π*	30.17	0.39	0.097
	O2	LP(2)	O1-C7	σ*	32.51	0.61	0.128
	O3	LP(2)	C8-C9	σ*	20.40	0.64	0.103
	N1	LP(2)	O3-C9	π*	69.55	0.26	0.123

	C1'-C2'	π	C3'-C4'	π*	20.29	0.31	0.070
	C3'-C4'	π	C5'-C6'	π*	21.13	0.28	0.069
	C5'-C6'	π	C1'-C2'	π*	21.15	0.29	0.070
	O1'	LP(2)	O2'-C7'	π*	30.17	0.39	0.097
	O2'	LP(2)	O1'-C7'	σ*	32.51	0.61	0.128
	O3'	LP(2)	C8'-C9'	σ*	20.40	0.64	0.103
	N1'	LP(2)	O3'-C9'	π*	69.55	0.26	0.123
	O3	LP(2)	N1'-H1A'	σ*	8.40	0.71	0.070
	O3'	LP(2)	N1-H1A	σ*	8.40	0.71	0.070
	O1	LP(1)	C8-H8	σ*	1.70	0.94	0.036
	O1'	LP(1)	C8'-H8'	σ*	1.70	0.94	0.036
6o	C1-C2	π	C3-C4	π*	23.75	0.28	0.074
	C3-C4	π	C5-C6	π*	20.59	0.29	0.071
	C5-C6	π	C1-C2	π*	21.97	0.29	0.072
	O1	LP(2)	O2-C7	π*	31.86	0.39	0.099
	O2	LP(2)	O1-C7	σ*	32.04	0.62	0.128
	O3	LP(2)	N1-C9	σ*	20.75	0.74	0.112
	N1	LP(1)	O3-C9	π*	64.54	0.27	0.120
	C1'-C2'	π	C3'-C4'	π*	23.75	0.28	0.074
	C3'-C4'	π	C5'-C6'	π*	20.59	0.29	0.071
	C5'-C6'	π	C1'-C2'	π*	21.97	0.29	0.072
	O1'	LP(2)	O2'-C7'	π*	31.86	0.39	0.099
	O2'	LP(2)	O1'-C7'	σ*	32.04	0.62	0.128
	O3'	LP(2)	N1'-C9'	σ*	20.75	0.74	0.112
	N1'	LP(1)	O3'-C9'	π*	64.54	0.27	0.120
	O3	LP(2)	N1'-H1A	σ*	6.55	0.70	0.062
	O3'	LP(2)	N1-H1A	σ*	6.55	0.70	0.062
	O1	LP(2)	C8-H8	σ*	2.87	0.72	0.042
	O1	LP(2)	C8'-H8'	σ*	2.87	0.72	0.042

It is evident from Table 5 that different types of non-covalent interactions (NCIs) are present in **5m**, **6e**, **6h** and **6o**. The intermolecular and intramolecular hydrogen bonding are the most attentive interactions among them. In the dimeric structure of **5m**, intermolecular hydrogen bonding is observed owning to the delocalization of the lone pair of O2LP(2) and O2'LP(2) to the antibonding sigma orbitals (σ*) of O1'-H1' and O1-H1 respectively. Consequently, the stabilization energy as 17.64 kcal/mol is offered to the dimeric **5m** structure by both hydrogen

bonds. Similarly, intramolecular HB offers 5.16 kcal/mol and 5.24 kcal/mol stabilization energy to the dimeric **5m** structure by delocalizing the lone pairs from O2LP(2) and O2'LP(1) to the σ* orbital of N1-H1A and N1'-H1A' respectively. In **6e,** intramolecular HB is endorsed by the transition in which effective delocalization of the lone pair of electron from O2LP(2) to the antibonding sigma orbitals (σ*) of C17-H18 is observed which leads to stabilization energy value of 2.84 kcal/mol. The dimeric structure **6h** likewise involves both intermolecular and intramolecular HBs. The intermolecular HB in **6h** is the result of delocalization of lone pair of electrons from O3LP(2) and O3'LP(2) to the σ* of N1'-H1A' and N1-H1A respectively. In these cases, the stabilization energy value is reported to be 8.40 kcal/mol respectively. The intramolecular HB in **6h** is evident from LP1(O1)→σ*(C8-H8) and LP1(O1')→σ*(C8'-H8') transitions which provide same stabilization energy value of 1.70 kcal/mol to the dimeric **6h** structure. The reasonable explanation to the presence of intermolecular and intramolecular hydrogen bonding interactions in **6o** dimeric structure is given by intermolecular transitions O3LP(2)→σ*(N1'–H1A), O3'LP(2)→σ*(N1–H1A) and intramolecular interactions O1LP(2)→σ*(C8–H8), O1'LP(2)→σ*(C8'–H8') respectively. The stabilization energy values 6.55 and 2.87 kcal/mol to the dimeric **6o** structure is given by above mentioned intermolecular and intramolecular transitions respectively. Apart from the HBs, delocalization of π-electrons from bonding orbitals of C-C to their anti-bonding orbitals play a key role for stabilization of rings and overall architecture. Thus existence of conjugation is well proven in **5m** from transitions π(C2–C7)→π*(C3–C4), π(C3–C4)→π*(C2–C7), π(C5–C6)→π*(C2–C7), π(C2'–C7')→π*(C3'–C4'), π(C3'–C4')→π*(C2'–C7') and π(C5'–C6')→π*(C2'–C7') with stabilization energy values 24.20, 14.92, 24.08, 24.20, 14.92 and 24.08 kcal/mol respectively. The existence of conjugation in **6e** is confirmed from π→π* interactions as π(C6–C15)→π*(C7–C9), π(C7–C9)→π*(C11–C13), π(C11–C13)→π*(C6–C15), π(C19–C20)→π*(C26–C28), π(C22–C24)→π*(C19–C20) and π(C26–C28)→π*(C19–C20) with substantial stabilization energy values 19.66, 21.62, 21.74, 20.18, 21.32 and 21.38 kcal/mol respectively. Similarly, the transitions π(C1–C2)→π*(C3–C4), π(C3–C4)→π*(C5–C6), π(C5–C6)→π*(C1–C2), π(C1'–C2')→π*(C3'–C4'), π(C3'–C4')→π*(C5'–C6') and π(C5'–C6')→π*(C1'–C2') with substantial stabilization energy values 20.29, 21.13, 21.15, 20.29, 21.13 and 21.15 kcal/mol respectively proved the presence of conjugation in **6h** dimeric structure. The delocalization of π-electrons

from bonding orbitals of C-C to their anti-bonding orbitals in **6o** is observed in π(C1–C2)→π*(C3–C4), π(C3–C4)→π*(C5–C6), π(C5–C6)→π*(C1–C2), π(C1'–C2')→π*(C3'–C4'), π(C3'–C4')→π*(C5'–C6') and π(C5'–C6')→π*(C1'–C2') transitions which offers stabilization energy values 23.75, 20.59, 21.97, 23.75, 20.59 and 21.97 kcal/mol respectively to the **6o** dimeric structure. The large stabilization energy values to the structure of investigated molecules **5m**, **6e**, **6h** and **6o** are offered in case of resonance. Some probable transitions noticed due to resonance in **5m** are O1(LP2)→π*(O2-C1), O2(LP1)→σ*(O1-C1), N1(LP1)→π*(C2-C7), O1'(LP2)→π*(O2'-C1'), O2'(LP1)→σ*(O1'-C1') and N1'(LP1)→π*(C2'-C7') with stabilization energy values 59.91, 20.53, 41.99, 59.91, 20.53 and 41.99 kcal/mol respectively. In **6e,** the large stabilization energy values 33.61, 32.13, 27.59 and 53.48 are offered by the resonance owing to O1(LP2)→π*(O2-C5), O2(LP2)→σ*(O1-C5), O3(LP2)→σ* (N4-C16) and N4(LP1)→π*(O3-C16) interactions respectively. Similarly, the transitions due to resonance observed in **6h** and **6o** are O1(LP2)→π*(O1-C7), O2(LP2)→σ*(O1-C7), O3(LP2)→σ*(C8-C9), N1(LP2)→π*(O3-C9), O1'(LP2)→π*(O1'-C7'), O2'(LP2)→σ*(O1'-C7'), O3'(LP2)→σ*(C8'-C9'), N1'(LP2)→π*(O3'-C9') and O1(LP2)→π*(O2-C7), O2(LP2)→σ*(O1-C7), O3(LP2)→σ*(N1-C9), N1(LP1)→π*(O3-C9), O1'(LP2)→π*(O2'-C7'), O2'(LP2)→σ*(O1'-C7'), O3'(LP2)→σ*(N1'-C9'), N1'(LP1)→π*(O3'-C9') with stabilization energy values 30.17, 32.51, 20.40, 69.55, 30.17, 32.51, 20.40, 69.55 and 31.86, 32.04, 20.75, 64.54, 31.86, 32.04, 20.75, 64.54 kcal/mol respectively. From preceding discussion**,** it can be concluded that presence of hydrogen bonding in investigated molecules **5m**, **6e**, **6h** and **6o** proves a good agreement between NBO and XRD findings. The extended conjugation is present in all compounds **5m**, **6e**, **6h** and **6o**. Successful intramolecular and intermolecular charge transfer due to delocalization of electrons on whole systems and hyper-conjugative interactions (HCIs) among bonds provide stability to the investigated compounds and are pivotal cause for the existence of investigated compounds **5m**, **6e**, **6h** and **6o** in the solid-state.

UV-Visible study

Ultraviolet-Visible (UV–Vis) spectroscopy is recognized as an important tool to describe the probability of charge transfer, contributing configurations to the transitions and electronic transition nature within the investigated molecules. Herein, photophysical characteristics of **5m**,

6e, **6h** and **6o** were explained by performing ultraviolet spectral characterization at B3LYP/6-311+G(d,p) level of theory. The calculated results of excitation energy (E^{DFT}), absorption wavelengths (λ_{max}), dominant molecular orbital (MO) contributions and oscillator strength (*f*) of **5m**, **6e**, **6h** and **6o** are collected in Table 6.

Table 6: Wave length, excitation energy and oscillator strength for **5m, 6e, 6h** and **6o**

Compound	Cal. λ_{max} (nm)	E^{DFT} (eV)	f	MO contributions
5m	329.21	3.7658	0.1368	H→L(95%)
	285.59	4.3410	0.0021	H-1→L(85%), H-1→L+1(11%)
	266.12	4.6586	0.2248	H-2→L(13%), H→L+1(84%)
	251.58	4.9279	0.0009	H-7→L(15%), H-6→L(30%), H-3→L(18%), H-1→L+1(30%)
	245.33	5.0535	0.0001	H→L+2(95%)
	243.49	5.0917	0.0005	H-6→L(15%), H-3→L(14%), H-1→L(12%), H-1→L+1(50%)
6e	297.32	4.1698	0.0955	H→L(94%)
	265.77	4.6647	0.0269	H-3→L(11%), H-2→L(12%), H-1→L(12%), H→L+1(48%)
	259.05	4.7858	0.0633	H-5→L(18%), H-2→L(14%), H-1→L(20%), H→L+1(35%)
	254.73	4.8669	0.0464	H→L+2(64%)
	253.46	4.8913	0.0101	H-3→L(20%), H-1→L(41%)
	247.33	5.0125	0.0253	H-1→L+2(17%),H→L+2(14%),H→L+3(46%)
6h	295.39	4.1970	0.0608	H→L(90%)
	266.82	4.6465	0.0114	H-3→L(21%), H-1→L(60%)
	253.29	4.8947	0.1388	H-3→L(21%),H-1→L+1(13%), H→L+1(49%)
	251.18	4.9357	0.0251	H-2→L(57%), H→L+1(16%)
	236.69	5.2379	0.0393	H-3→L(16%), H-2→L(11%), H-2→L+1(22%), H-1→L(13%), H-1→L+1(20%)
	223.16	5.5555	0.2885	H-3→L(18%), H-2→L(14%), H-1→L+1(19%), H→L+1(13%), H→L+2(15%)
6o	305.69	4.0556	0.0565	H→L(91%)
	271.48	4.5667	0.0112	H-3→L(21%), H-1→L(58%), H→L+1(10%),
	267.99	4.6262	0.0005	H→L+2(97%)
	258.99	4.7869	0.1846	H-3→L(14%), H→L+1(62%)
	256.46	4.8342	0.0001	H-3→L(12%), H-2→L(56%), H-2→L+1(12%)
	243.87	5.0836	0.0171	H-3→L(21%), H-2→L+1(25%), H-1→L(15%), H-1→L+1(18%)

E = Excitation energy (eV); λ=wave length (nm); *f* = oscillator strength; MO = molecular orbitals; H = HOMO, L = LUMO; λ (nm) Cal. = Calculated.

Results indicate that first vertical transition is found to be as major transitions having maximum absorption values appeared at 329.21 nm, 297.32 nm, 295.39 nm and 305.69 nm originated from HOMO→LUMO (95%), HOMO→LUMO (94%), HOMO→LUMO (90%) and HOMO→ LUMO (91%) of **5m**, **6e**, **6h** and **6o** respectively. Due to minute structural difference, calculated absorption maxima (λ_{max}) values are found very close to each other. Overall, highest vertical transition among all investigated molecules is observed in **5m** with absorption value 329.21 nm. Compound **6o** is placed at second position, while **6e** and **6h** hold the third and fourth positions in terms of maximum absorption values observed in all vertical transitions. The decreasing order of λ_{max} values are noted as: **5m** > **6o** > **6e** > **6h.** This order is exactly inverse to the HOMO-LUMO gap order **5m** < **6o** < **6e** < **6h** which indicate that molecule with less energy gaps are shifted towards longer wavelength. It can also be seen from Table 6 that wavelengths 266.12 nm, 297.32 nm, 223.16 nm and 258.99 nm in compounds **5m, 6e**, **6h** and **6o** are observed with maximum oscillator strength values of 0.2248, 0.0955, 0.2885 and 0.1846 respectively.

Another important factor that offers useful insights into the charge transfer character is transition or excitation energy of investigated molecules. Literature suggests that molecules holding lower transition energy values contain higher charge transport ability and easy excitation between HOMO to LUMO. The increasing order for E^{DFT} values are found to be:

[**5m** (3.7658 *eV*)] < [**6o** (4.0556 *eV*)] < [**6e** (4.1698 *eV*)] < [**6h** (4.1970*eV*)]

This increasing order is also found in accordance with the HOMO-LUMO gap order describing the reasons for shifting in absorption maximum toward longer wavelength. The MO contribution also indicates that maximum intramolecular charge in **5m, 6e**, **6h** and **6o** are transferred from HOMO to LUMO electronic transition which is the characteristic of soft molecules, hence, may have potential of utilization in biological and NLO applications.

Frontier molecular orbital (FMO) analysis

Different characteristics including molecular interactions, reactivity, charge transfer, optical properties and electronic features of molecules under investigation are studied using frontier molecular orbitals (FMOs) namely highest occupied molecular orbital (HOMO) and lowest unoccupied molecular orbital (LUMO) [40, 41]. These FMOs take the responsibility of any

chemical reaction. The HOMO is designated as an electron donor, while LUMO is assigned for acceptance of the electron. The molecular chemical stability can be defined through the energy gap between HOMO and LUMO ($\Delta E = E_{LUMO}$-E_{HOMO}). The molecular electrical transport properties can be determined using energy gap of frontier molecular orbitals [42]. The bonding framework of investigated molecules is elucidated through the surface of FMOs. Hence, two paramount molecular orbital pairs HOMO, HOMO-1 and LUMO, LUMO+1, which reflect both the donor and acceptor levels, one energy state above LUMO and one level below HOMO for **5m, 6e**, **6h** and **6o** respectively are examined. The pictorial representation is shown in Figure 7 in which red color specifies the negative phase while green color indicates the positive phase of molecular orbitals respectively. The energy data for four molecular orbitals of **5m, 6e**, **6h** and **6o** along with their energy differences are shown in Table 7.

Table 7: Computed energies (E) for compounds **5m**, **6e**, **6h** and **6o**.

MO(s)	**5m**		**6e**		**6h**		**6o**	
	E (*eV*)	ΔE (*eV*)	E (*eV*)	ΔE (*eV*)	E (*eV*)	ΔE (*eV*)	E (*eV*)	ΔE (*eV*)
HOMO	-6.747	4.302	-6.671	4.836	-6.938	4.846	-7.109	4.714
LUMO	-2.445		-1.835		-2.092		-2.395	
HOMO-1	-7.687	6.142	-7.329	6.048	-7.685	6.192	-7.815	6.002
LUMO+1	-1.545		-1.281		-1.493		-1.813	

E = energy, Δ*E* (e*V*) = E_{LUMO} - E_{HOMO}; HOMO = highest occupied molecular orbital; LUMO = lowest unoccupied molecular orbital; MO = molecular orbital

The energy for four molecular orbitals (HOMO, LUMO, HOMO-1, LUMO+1) of **5m**, **6e**, **6h** and **6o** are found to be negative which indicates that investigated molecules are stable [43]. The energy gaps values of **6e** and **6h** are found close to each other with only a third digit difference. The smallest energy gap value among investigated compounds (**5m**, **6e**, **6h** and **6o)** is found to be in **5m** with ΔE value of 4.302 eV. This might due to the presence of two weakly deactivating Cl and Br groups at opposite ends of the **5m** architecture. In contrast, computational findings reflect that the highest ΔE value of 4.846 eV is observed in **6h.** Overall, the increasing order of HOMO-LUMO energy gap is noticed as: **5m** <**6o** <**6e** < **6h.**

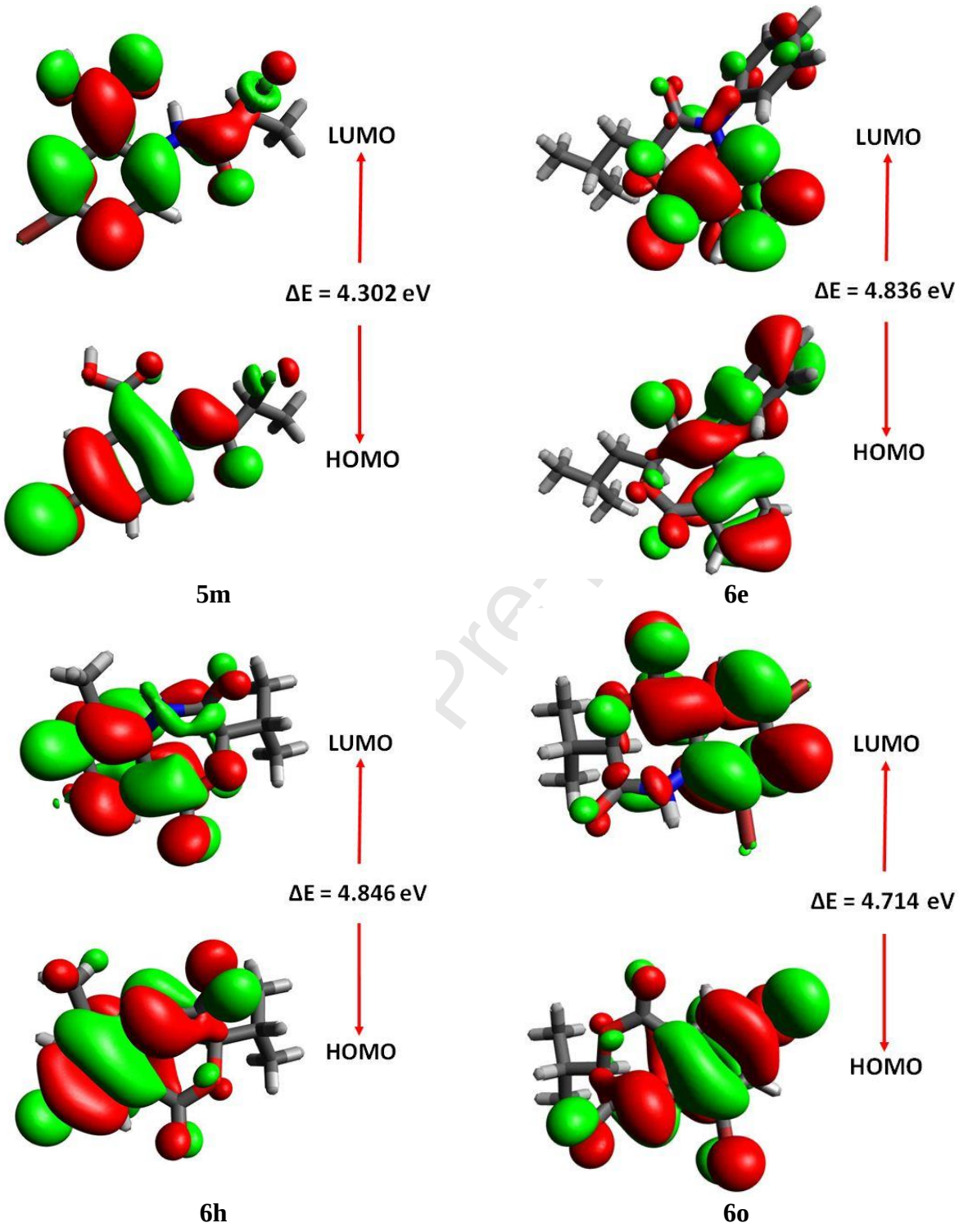

Figure 7. Frontier molecular orbitals of **5m, 6e, 6h** and **6o**

Global reactivity parameters [44-47] are helpful to interpret the stability, chemical reactivity and internal charge transfer of investigated compounds. Therefore energies of FMOs and their gaps

are used to estimate these parameters. First, ionization potential (*I*) and electron affinity (*A*) values of **5m, 6e, 6h** and **6o** were calculated in vertical manner employing equations 6 and 7.

$$I = E_c^{N-1} - E_o^N \quad \text{Equation (6)}$$

$$A = E_o^N - E_A^{N+1} \quad \text{Equation (7)}$$

The I represent the ionization potential while A indicates the electron affinity values. The E_c^{N-1} and E_A^{N+1} factors describe the energy after losing (cation) and gaining an electron (anion) respectively. The E_o^N is the basal state energy (neutral).

Chemical hardness (η), electronegativity (X), electrophilicity (ω) calculations including electron donating (ω^-) or electron accepting ability (ω^+) of chemical specie and softness values (σ) of **5m, 6e, 6h** and **6o** are calculated using equations 8-13 respectively.

$$\eta = \frac{I-A}{2} \quad \text{Equation (8)}$$

$$X = \frac{I+A}{2} \quad \text{Equation (9)}$$

$$\omega = \frac{\mu^2}{2\eta} \quad \text{Equation (10)}$$

$$\omega^- = \frac{(3I + A)^2}{16 (I - A)} \quad \text{Equation (11)}$$

$$\omega^+ = \frac{(I + 3A)^2}{16 (I - A)} \quad \text{Equation (12)}$$

$$\sigma = \frac{1}{2\eta} \quad \text{Equation (13)}$$

The results obtained from equations 2-9 are presented in Table 8.

Table 8: Ionization potential (I), electron affinity (A), electronegativity (X), global hardness (η), chemical potential (μ), global electrophilicity (ω), electron donor capability (ω^-), electron acceptor capability (ω^+) and global softness (σ).

	I	**A**	**X**	**η**	**μ**	**ω**	**ω^-**	**ω^+**	**σ**
5m	8.38	0.86	4.62	3.76	-4.62	2.84	5.62	0.99	0.13
6e	8.15	0.30	4.22	3.92	-4.22	2.27	4.88	0.65	0.12
6h	8.57	0.47	4.52	4.05	-4.52	2.53	5.30	0.77	0.12
6o	8.68	0.82	4.75	3.92	-4.75	2.87	5.74	0.98	0.12

The *A* and *I* values are directly related to the electron accepting and donating character of LUMO and HOMO respectively. The *I* values of **5m, 6e, 6h** and **6o** are found larger than corresponding *A* values indicating the greater electron donating aptitude of **5m, 6e, 6h** and **6o** as compared to their accepting nature. The highest *A* values is noticed in **5m** indicating its greater reactivity and least stability as compared to other investigated compounds. Overall, *A* value is found positive in all compounds which is a good indication for the possible utilization of these compounds in charge transfer reactions. Electrophilicity results also evident that electron donor capability (ω^-) values of **5m, 6e, 6h** and **6o** are very large as compared to the electron accepting capability (ω^+) values. The global softness value is found to be similar (0.12 E_h) in **6e, 6h** and **6o,** while one digit greater as 0.13 E_h in compound **5m** indicating the better reactivity and less stability of **5m** as compared to other studied compounds. The least value of global hardness (3.76 E_h) is found to be in **5m** describing the less stability and greater reactivity of **5m** as compared to other investigated compounds. Table 8 also uncovers that the magnitude of hardness is greater than softness in all compounds, which means that all studied molecules hold high stability. Overall, the increasing order of global hardness values is noticed as: **5m** <**6o** <**6e** < **6h.** This order is in fine agreement with the HOMO-LUMO energy gap proving the fact that molecules with large ΔE value are considered as hard molecules with greater kinetic stability, less reactivity and resistance to change in electronic configurations. The negative chemical potential discloses the stability of the systems. The negative magnitude of chemical potential also provides strengthen to the stability and inclination towards decomposition into its elements cannot be possible easily with the exception of external force. Overall findings of global reactivity parameters indicate that all investigated compounds contain more donating capability, stability and less accepting aptitude. All studied compounds are suitable and can participate in charge transfer reactions. Furthermore, investigated compounds have the ability to play the role in optoelectronic technologies.

Nonlinear optical (NLO) properties

The expansion of materials regarding NLO characteristics exploration is an area of frontier research owing to their versatile applications in enhanced data rates, frequency mixing and harmonic generation associated with the technology of potential communication [48-51]. Non-

centrosymmetric architectures possess NLO character due to intramolecular charge transfer (ICT) and delocalization of electrons. Non-centrosymmetric architecture can be attained by suitable substitution of electron donor and acceptor units on basic backbone of the molecules which leads to the designing of efficient NLO materials [52-57]. To explore the potential NLO features of **5m, 6e, 6h** and **6o**, computational calculations have been performed at B3LYP/6311+G(d,p) level of DFT. Average polarizability (α), first hyperpolarizability (β_{tot}) and second hyperpolarizability $\langle\gamma\rangle$ values of **5m, 6e, 6h** and **6o** are calculated using equations 14-16 and results are collected in Tables 9-11.

$$<\alpha>=1/3(\alpha_{xx}+\alpha_{yy}+\alpha_{zz}) \qquad \text{Equation (14)}$$

$$\beta_{tot}=[(\beta_{xxx}+\beta_{xyy}+\beta_{xzz})^2+(\beta_{yyy}+\beta_{xxy}+\beta_{yzz})^2+(\beta_{zzz}+\beta_{xxz}+\beta_{yyz})^2]^{1/2} \qquad \text{Equation (15)}$$

$$\langle\Upsilon\rangle=\frac{1}{5}\left(\Upsilon_{xxxx}+\Upsilon_{yyyy}+\Upsilon_{zzzz}+2[\Upsilon_{xxyy}+\Upsilon_{yyzz}+\Upsilon_{xxzz}]\right) \qquad \text{Equation (16)}$$

Table 9: The dipole moment (D) and computed dipole polarizabilities (a.u.) for **5m**, **6e**, **6h** and **6o**.

	μ_x	μ_y	μ_z	μ	α_{xx}	α_{yy}	α_{zz}	α_{total} **(a.u)**
5m	-0.2888	2.0805	-1.7359	2.7250	253.66	174.44	108.28	178.80
6e	-2.4652	1.5070	-4.3015	5.1818	268.79	254.42	188.99	237.40
6h	1.4521	3.6783	2.9784	4.9506	240.33	189.49	125.14	184.99
6o	1.4546	1.5977	2.9740	3.6760	259.56	216.96	132.03	202.85

Table 10: The computed first hyperpolarizability/second order NLO (a.u.) for **5m**, **6e**, **6h** and **6o**

	β_{xxx}	β_{xxy}	β_{xyy}	β_{yyy}	β_{xxz}	β_{yyz}	β_{xzz}	β_{yzz}	β_{zzz}	β_{tot} **(a.u)**
5m	572.502	-171.799	113.874	350.181	-7.47847	-18.8571	-66.7717	-25.1448	-6.16861	639.099
6e	-65.8494	-45.8141	102.574	433.379	4.69244	-69.5675	7.55460	-17.5839	-112.681	412.763
6h	-219.139	-40.2700	-0.84705	21.7769	0.07546	-13.2829	-1.52927	28.8880	66.4016	228.050
6o	-133.320	-56.1222	20.5088	-31.1057	7.17297	6.4556	38.0880	15.2879	90.8122	147.196

Table 11: The second hyperpolarizability values (a.u.) for **5m**, **6e**, **6h** and **6o**

	γ_{xxxx}	γ_{yyyy}	γ_{zzzz}	γ_{xxyy}	γ_{zzxx}	γ_{yyzz}	$\langle\gamma\rangle$ **(a.u.)**
5m	-6562.45	-1254.86	-334.942	-1419.130	-1184.46	-317.493	-9320.69
6e	-6215.90	-2881.10	-1000.085	-1553.32	-1247.60	-674.03	-11487.07
6h	-5037.25	-1719.97	-644.496	-1144.64	-968.368	-422.150	-8415.79
6o	-5934.87	-2665.61	-687.932	-1488.31	-1134.25	-610.014	-10581.45

The relative analysis of dipole moments mentioned in Table 9 showed that charge distribution takes place along x, y and z directions for **5m, 6e, 6h** and **6o**. The highest and lowest dipole moment values among all investigated molecules **5m, 6e, 6h** and **6o** are found to be 5.1818 D and 2.7250 in **6e** and **5m** respectively. The dipole moment values denote that there is a definite distance between different atoms of **5m, 6e, 6h** and **6o** which leads to the polarization, hence, NLO response properties. The dipole moment of **5m, 6e, 6h** and **6o** are also compared with the urea molecule which is frequently studied as standard for comparison of first hyperpolarizability and dipole moment values. Dipole moment values of **5m, 6e, 6h** and **6o** are found to be 1.98, 3.77, 3.60 and 2.76 times greater than dipole moment of urea molecule (1.3732 D) [58].

In case of linear polarizability, the data mentioned in Table 9 show that polarizability tensor along x-axis is more dominant among all polarizability tensors of **5m, 6e, 6h**, **6o,** and its contribution towards total linear polarizability is more pronounced than others. The highest linear polarizability value (237.40 a.u) among all investigated molecules **5m, 6e, 6h** and **6o** is shown by **6e** while lowest linear polarizability value 178.80 a.u is found in **5m**. The decreasing order of linear polarizability values is **6e** > **6o** > **6h** > **5m.**

In case of first hyperpolarizability (β_{tot}), the dominant contribution to β_{tot} is made by x-axis direction transition with positive values (572.502 a.u) in **5m**, while with negative values (-219.139 a.u and -133.320 a.u) in **6h** and **6o** respectively. In case of **6e**, y-axis tensor with positive value of 433.379 a.u is found to be responsible for dominant contribution towards β_{tot}. The larger hyperpolarizability values are shown by molecules with smallest energy gap and large global softness values. This statement also exists in our studied systems where **5m** with smallest energy gap and largest softness value among all investigated molecules showed the highest β_{tot} value 639.099 (a.u). The lowest β_{tot} value of is found to be 147.196 a.u in **6o**. The decreasing order of β_{tot} values is found to be **5m** > **6e** > **6h** > **6o**. NLO findings were further compared with standard urea molecule which indicate that β_{tot} values of **5m**, **6e**, **6h** and **6o** are marked 14.86, 9.59, 5.30 and 3.42 times larger than β_{tot} value of urea=43 a.u [58]. The values of second hyperpolarizability <**γ**> along with their contributing tensors are presented in Table 10. The <**γ**> values of **5m**, **6e**, **6h** and **6o** are found to be -9320.69 (a.u.) and -11487.07 (a.u.), -8415.79 (a.u.) and -10581.45 (a.u.) respectively.

Overall findings indicate that all investigated molecules **5m**, **6e**, **6h** and **6o** hold polarizable nature. The urea molecule comparative analysis proposed that all investigated molecules **5m**, **6e**, **6h** and **6o** are appropriate NLO candidates. Particularly **5m** with highest global softness, lowest energy gap and highest first hyperpolarizability values wins the contest and may have prospective uses in the technology related applications

Conclusion

The comparison of cyclization reaction of *N*-acyl anthranilic acid **5a-p** to 4,1-benzoxazepines **6a-p** via conventional method versus MW assisted revealed that conventional heating method afforded4,1-benzoxazepines in low yields and longtime duration (3 h). Whereas, MW assisted cyclization of *N*-acyl anthranilic acid is nippiest method for accomplishment of final 4,1-benzoxazepines in divergence to conventional heating method. Herein, four novel compounds with chemical formulas $C_{10}H_9BrClNO_3$ (**5m**), $C_{19}H_{19}NO_3$ (**6e**), $C_{13}H_{14}ClNO_3$ (**6h**) and $C_{12}H_{11}Br_2NO_3$ (**6h**) were synthesized and confirmed using SC-XRD study which disclosed that **5m** and **6o** crystallize in triclinic crystal lattice with $P\bar{1}$ space group, **6e** in orthorhombic crystal lattice with *Pbca* space group and **6h** crystallize in monoclinic crystal lattice with $P2_1/c$ space group. The geometrical parameters and experimental FT-IR spectroscopic analysis showed reasonable agreement to corresponding DFT based geometrical parameters and FT-IR vibrations. Presence of hydrogen bonding in **5m**, **6e**, **6h** and **6o** proves a good agreement between NBO analysis and XRD findings. The NBO analysis confirmed that the presence of non-covalent interactions, hydrogen bonding, hyper-conjugative interactions, intramolecular and intermolecular charge transfer are pivotal cause for the existence of **5m**, **6e**, **6h** and **6o** in the solid-state. The decreasing order of λ_{max} values are noted (as **5m** > **6o** > **6e** > **6h)** exactly inverse to the HOMO-LUMO gap order **5m** <**6o** < **6e** < **6h** which indicate that molecule with less energy gaps are shifted towards longer wavelength. Global reactivity parameters indicate that **5m**, **6e**, **6h** and **6o** contain more donating capability, stability and less accepting aptitude. NLO analysis confirmed that all studied compounds (**5m**, **6e**, **6h** and **6o)** especially **5m** with highest global softness (0.13 E_h), lowest energy gap (4.302 eV) and highest first hyperpolarizability (639.099 a.u) values have significant NLO properties as compared to prototype standard compound which disclosed their potential for technology related applications. We hope that this synergistic

experimental-computational study may provide new ways for the utilization of **5m**, **6e**, **6h** and **6o** in supramolecular chemistry and as NLO material for optoelectronic applications.

Acknowledgement

The authors are highly obliged to the Higher Education Commission (HEC) of Pakistan for fellowship and IRSIP award to Bushra Nisar and payment for spectral analysis (NMR and MS) of the synthesized compounds. We are also thankful to the Dr Irshad Hussain and Lahore University of Management Sciences (LUMS), Lahore (Pakistan) for sharing microwave reactor. Ataualpa A. C. Braga, (grants # 2011/07895-8, 2015/01491-3 and 2014/25770-6) is thankful to Fundação de Amparo à Pesquisa do Estado de São Paulo for financial support. AACB (grant 309715/2017-2) also thanks the Brazilian National Research Council (CNPq) for financial support and fellowships. This study was financed in part by the Coordenação de Aperfeiçoamento de Pessoal de Nível Superior – Brazil (CAPES) – Finance Code 001.

Conflict of interest

No conflicts declared.

References

[1] M. Pastó, B. Rodríguez, A. Riera, M.A. Pericas, Synthesis of enantiopure amino alcohols by ring-opening of epoxyalcohols and epoxyethers with ammonia, Tetrahedron Lett. 44(46) (2003) 8369-8372.
[2] U.M. Lindström, B. Olofsson, P. Somfai, Microwave-assisted aminolysis of vinylepoxides, Tetrahedron Lett. 40(52) (1999) 9273-9276.
[3] S.-M. Nathwani, S. Butler, D. Fayne, N.N. McGovern, B. Sarkadi, M.J. Meegan, D.G. Lloyd, G. Campiani, M. Lawler, D.C. Williams, Novel microtubule-targeting agents, pyrrolo-1, 5-benzoxazepines, induce apoptosis in multi-drug-resistant cancer cells, Cancer Chemother. Pharmacol. 66(3) (2010) 585-596.
[4] H. Agirbas, B. Kemal, F. Budak, Synthesis and structure–antibacterial activity relationship studies of 4-substituted phenyl-4, 5-dihydrobenzo [f][1, 4] oxazepin-3 (2H)-thiones, Med. Chem. Res. 20(8) (2011) 1170-1180.
[5] E. Lichtfouse, J. Schwarzbauer, D. Robert, Environmental chemistry for a sustainable world: volume 2: remediation of air and water pollution, Springer Science & Business Media2011.
[6] C.G. Neochoritis, C.A. Tsoleridis, J. Stephanidou-Stephanatou, C.A. Kontogiorgis, D.J. Hadjipavlou-Litina, 1, 5-Benzoxazepines vs 1, 5-benzodiazepines. One-pot microwave-assisted synthesis and evaluation for antioxidant activity and lipid peroxidation inhibition, J. Med. Chem. 53(23) (2010) 8409-8420.
[7] H. Kwiecien, M. Smist, A. Wrzesniewska, Synthesis of aryl-fused 1, 4-oxazepines and their oxo derivatives: A Review, Current Organic Synthesis 9(6) (2012) 828-850.

[8] J. Przytocka-Balik, B. Bobrański, New derivatives of 2, 4-diketo-1, 2, 4, 5-tetrahydro-3H-benzoxazepine [1, 5] and 2, 4-diketo-2, 3-dihydro-4H-benzodioxepine [1, 5], Il Farmaco; edizione scientifica 33(5) (1978) 360.
[9] M. Yar, E.M. McGarrigle, V.K. Aggarwal, Bromoethylsulfonium Salt瑿 A More Effective Annulation Agent for the Synthesis of 6-and 7-Membered 1, 4-Heterocyclic Compounds, Org. Lett. 11(2) (2008) 257-260.
[10] R.A. Glennon, R. Young, Drug discrimination: applications to medicinal chemistry and drug studies, John Wiley & Sons2011.
[11] B. Nisar, A.R. Raza, D.S. Black, N. Kumar, M.N. Tahir, Stereoselective Synthesis of (3R)-3-Alkyl-4, 1-Benzoxazepine-2, 5-Diones, Chirality 25(12) (2013) 865-870.
[12] S. Rubab, B. Nisar, A. Raza, N. Ullah, M. Tahir, Asymmetric Synthesis of 4, 1-Benzoxazepine-2, 5-Diones—Effect of the Halogen of (2S)-α-Haloacids, Molecules 19(1) (2014) 139-148.
[13] Ghiasuddin, M. Akram, M. Adeel, M. Khalid, M.N. Tahir, M.U. Khan, M.A. Asghar, M.A. Ullah, M. Iqbal, A combined experimental and computational study of 3-bromo-5-(2, 5-difluorophenyl) pyridine and 3, 5-bis (naphthalen-1-yl) pyridine: Insight into the synthesis, spectroscopic, single crystal XRD, electronic, nonlinear optical and biological properties, J. Mol. Struct. 1160 (2018) 129-141.
[14] M.S. Ahmad, M. Khalid, M.A. Shaheen, M.N. Tahir, M.U. Khan, A.A.C. Braga, H.A. Shad, Synthesis and XRD, FT-IR vibrational, UV–vis, and nonlinear optical exploration of novel tetra substituted imidazole derivatives: A synergistic experimental-computational analysis, J. Phys. Chem. Solids 115 (2018) 265-276.
[15] M. Shahid, M. Salim, M. Khalid, M.N. Tahir, M.U. Khan, A.A.C. Braga, Synthetic, XRD, non-covalent interactions and solvent dependent nonlinear optical studies of Sulfadiazine-Ortho-Vanillin Schiff base:(E)-4-((2-hydroxy-3-methoxy-benzylidene) amino)-N-(pyrimidin-2-yl) benzene-sulfonamide, J. Mol. Struct. 1161 (2018) 66-75.
[16] R. Jawaria, M. Hussain, M. Khalid, M.U. Khan, M.N. Tahir, M.M. Naseer, A.A.C. Braga, Z. Shafiq, Synthesis, crystal structure analysis, spectral characterization and nonlinear optical exploration of potent thiosemicarbazones based compounds: A DFT refine experimental study, Inorg. Chim. Acta 486 (2019) 162-171.
[17] M. Khalid, M.A. Ullah, M. Adeel, M.U. Khan, M.N. Tahir, A.A.C. Braga, Synthesis, crystal structure analysis, spectral IR, UV–Vis, NMR assessments, electronic and nonlinear optical properties of potent quinoline based derivatives: Interplay of experimental and DFT study, J. Saudi Chem. Soc. 23(5) (2019) 546–560.
[18] M.N. Tahir, S.H. Mirza, M. Khalid, A. Ali, M.U. Khan, A.A.C. Braga, Synthesis, single crystal analysis and DFT based computational studies of 2, 4-diamino-5-(4-chlorophenyl)-6-ethylpyrim idin-1-ium 3, 4, 5-trihydroxybenzoate-methanol (DETM), J. Mol. Struct. 1180 (2019) 119-126.
[19] M. Haroon, M. Khalid, T. Akhtar, M.N. Tahir, M.U. Khan, M. Saleem, R. Jawaria, Synthesis, spectroscopic, SC-XRD characterizations and DFT based studies of ethyl2-(substituted-(2-benzylidenehydrazinyl)) thiazole-4-carboxylate derivatives, J. Mol. Struct. 1187 (2019) 164-171.
[20] M. Rafiq, M. Khalid, M.N. Tahir, M.U. Ahmad, M.U. Khan, M.M. Naseer, A.A.C. Braga, S. Muhammad, Z. Shafiq, Synthesis, XRD, spectral (IR, UV–Vis, NMR) characterization and quantum chemical exploration of benzoimidazole-based hydrazones: A synergistic experimental-computational analysis, Appl. Organomet. Chem. (2019) e5182.
[21] B. Khan, M. Khalid, M.R. Shah, M.N. Tahir, M.U. Khan, A. Ali, S. Muhammad, Efficient Synthesis by Mono-Carboxy Methylation of 4, 4′-Biphenol, X-ray Diffraction, Spectroscopic Characterization and Computational Study of the Crystal Packing of Ethyl 2-((4′-hydroxy-[1, 1′-biphenyl]-4-yl) oxy) acetate, ChemistrySelect 4(32) (2019) 9274-9284.
[22] A. Hussain, M.U. Khan, M. Ibrahim, M. Khalid, A. Ali, S. Hussain, M. Saleem, N. Ahmad, S. Muhammad, A.G. Al-Sehemi, Structural parameters, electronic, linear and nonlinear optical exploration

of thiopyrimidine derivatives: A comparison between DFT/TDDFT and experimental study, J. Mol. Struct. 1201 (2020) 127183.
[23] A.A. Braga, G. Ujaque, F. Maseras, A DFT Study of the full catalytic cycle of the suzuki-miyaura cross-coupling on a model system, Organometallics 25(15) (2006) 3647-3658.
[24] M. García-Melchor, A.A. Braga, A. Lledós, G. Ujaque, F. Maseras, Computational perspective on Pd-catalyzed C–C cross-coupling reaction mechanisms, Acc. Chem. Res. 46(11) (2013) 2626-2634.
[25] A.A. Braga, N.H. Morgon, G. Ujaque, F. Maseras, Computational characterization of the role of the base in the Suzuki-Miyaura cross-coupling reaction, J. Am. Chem. Soc. 127(25) (2005) 9298-9307.
[26] M.J. Frisch, G.W. Trucks, H.B. Schlegel, G. Scuseria, M.A. Robb, J.R. Cheeseman, G. Scalmani, V. Barone, B. Mennucci, G. Petersson, H. Nakatsuji, M. Caricato, X. Li, H.P. Hratchian, A.F. Izmaylov, J. Bloino, G. Zheng, J.L. Sonnenberg, M. Hada, M. Ehara, K. Toyota, R. Fukuda, J. Hasegawa, M. Ishida, T. Nakajima, Y. Honda, O. Kitao, H. Nakai, T. Vreven, J.A. Montgomery, J.E. Peralta, F. Ogliaro, M. Bearpark, J.J. Heyd, E. Brothers, K.N. Kudin, V.N. Staroverov, R. Kobayashi, J. Normand, K. Raghavachari, A. Rendell, J.C. Burant, S.S. Iyengar, J. Tomasi, M. Cossi, N. Rega, J.M. Millam, M. Klene, J.E. Knox, J.B. Cross, V. Bakken, C. Adamo, J. Jaramillo, R. Gomperts, R.E. Stratmann, O. Yazyev, A.J. Austin, R. Cammi, C. Pomelli, J.W. Ochterski, R.L. Martin, K. Morokuma, V.J. Zakrzewski, G.A. Voth, P. Salvador, J.J. Dannenberg, S. Dapprich, A.D. Daniels, O. Farkas, J.B. Foresman, J.V. Ortiz, J. Cioslowski, D.J. Fox, D. 0109, Revision D. 01, Gaussian, Inc., Wallingford, CT (2009).
[27] F. Weinhold, E.D. Glendening, NBO 5.0 program manual: natural bond orbital analysis programs, Theoretical Chemistry Institute and Department of Chemistry, University of Wisconsin, Madison, WI 53706 (2001).
[28] R. Dennington, T. Keith, J. Millam, GaussView, version 5, Semichem Inc., Shawnee Mission, KS (2009).
[29] M.D. Hanwell, D.E. Curtis, D.C. Lonie, T. Vandermeersch, E. Zurek, G.R. Hutchison, Avogadro: an advanced semantic chemical editor, visualization, and analysis platform, J. Cheminform. 4(1) (2012) 17.
[30] ChemCraft, https://www.chemcraftprog.com/.
[31] B. Koppenhoefer, V. Schurig, (S)-2-Chloroalkanoic Acids of High Enantiomeric Purity from (S)-2-Amino Acides-(S)-2-Chloropropanoic Acid, Organic Syntheses 66 (1988) 151-159.
[32] J. Bernstein, R.E. Davis, L. Shimoni, N.L. Chang, Patterns in hydrogen bonding: functionality and graph set analysis in crystals, Angew. Chem. Int. Ed. Engl. 34(15) (1995) 1555-1573.
[33] G. Socrates, Infrared and Raman characteristic group frequencies: table and charts, Ltd WJS (2001) 1-347.
[34] H.H. Perkampus, LJ Bellamy: The Infrared Spectra of Complex Molecules, Vol. 1, 3. Auflage, Chapman and Hall Ltd., London 1975, 433 Seiten, 32 Abb., 22 Tabellen, Preis:£ 8.—, Ber. Bunsenges. Phys. Chem. 80(1) (1976) 99-100.
[35] D. Sathiyanarayanan, Vibrational Spectroscopy Theory and Application, New Age International Publishers, New Delhi (2004).
[36] R. Lu, W. Gan, B.-h. Wu, Z. Zhang, Y. Guo, H.-f. Wang, C− H stretching vibrations of methyl, methylene and methine groups at the vapor/alcohol (n= 1− 8) interfaces, J. Phys. Chem. B 109(29) (2005) 14118-14129.
[37] M. Szafran, A. Komasa, E. Bartoszak-Adamska, Crystal and molecular structure of 4-carboxypiperidinium chloride (4-piperidinecarboxylic acid hydrochloride), J. Mol. Struct. 827(1) (2007) 101-107.
[38] C. James, A.A. Raj, R. Reghunathan, V. Jayakumar, I.H. Joe, Structural conformation and vibrational spectroscopic studies of 2, 6-bis (p-N, N-dimethyl benzylidene) cyclohexanone using density functional theory, J. Raman Spectrosc. 37(12) (2006) 1381-1392.

[39] M. Snehalatha, C. Ravikumar, I.H. Joe, N. Sekar, V. Jayakumar, Spectroscopic analysis and DFT calculations of a food additive Carmoisine, Spectrochim. Acta. A Mol. Biomol. Spectrosc. 72(3) (2009) 654-662.
[40] M. Srnec, E.I. Solomon, Frontier Molecular Orbital Contributions to Chlorination versus Hydroxylation Selectivity in the Non-Heme Iron Halogenase SyrB2, J. Am. Chem. Soc. 139(6) (2017) 2396-2407.
[41] F. Kandemirli, S. Sagdinc, Theoretical study of corrosion inhibition of amides and thiosemicarbazones, Corros. Sci. 49(5) (2007) 2118-2130.
[42] M.U. Khan, J. Iqbal, M. Khalid, R. Hussain, A.A.C. Braga, M. Hussain, S. Muhammad, Designing triazatruxene-based donor materials with promising photovoltaic parameters for organic solar cells, RSC Adv. 9(45) (2019) 26402-26418.
[43] S. Xia, X. Xu, yl Sun, yl Fan, yH Fan, CF Bi, dM Zhang, lr yang, Chin. J. Struct. Chem 25 (2006) 849.
[44] R.G. Parr, L.v. Szentpaly, S. Liu, Electrophilicity index, J. Am. Chem. Soc. 121(9) (1999) 1922-1924.
[45] R.G. Parr, R.A. Donnelly, M. Levy, W.E. Palke, Electronegativity: the density functional viewpoint, J. Chem. Phys. 68(8) (1978) 3801-3807.
[46] P.K. Chattaraj, U. Sarkar, D.R. Roy, Electrophilicity index, Chem. Rev. 106(6) (2006) 2065-2091.
[47] A. Lesar, I. Milošev, Density functional study of the corrosion inhibition properties of 1, 2, 4-triazole and its amino derivatives, Chem. Phys. Lett. 483(4) (2009) 198-203.
[48] S. Muhammad, M.R.S.A. Janjua, Z. Su, Investigation of dibenzoboroles having π-electrons: toward a new type of two-dimensional NLO molecular switch?, J. Phys. Chem. C 113(28) (2009) 12551-12557.
[49] C.-G. Liu, Z.-M. Su, X.-H. Guan, S. Muhammad, Redox and photoisomerization switching the second-order nonlinear optical properties of a tetrathiafulvalene derivative across six states: a DFT study, J. Phys. Chem. C 115(48) (2011) 23946-23954.
[50] S. Muhammad, A. Irfan, A.G. Al-Sehemi, M. Al-Assiri, A. Kalam, A.R. Chaudhry, Quantum chemical investigation of spectroscopic studies and hydrogen bonding interactions between water and methoxybenzeylidene-based humidity sensor, J. Theor. Comput. Chem. 14(04) (2015) 1550029.
[51] S. Muhammad, C. Liu, L. Zhao, S. Wu, Z. Su, A theoretical investigation of intermolecular interaction of a phthalimide based "on–off" sensor with different halide ions: tuning its efficiency and electro-optical properties, Theor. Chem. Acc. 122(1-2) (2009) 77-86.
[52] M.U. Khan, M. Khalid, M. Ibrahim, A.A.C. Braga, M. Safdar, A.A. Al-Saadi, M.R.S.A. Janjua, First Theoretical Framework of Triphenylamine–Dicyanovinylene-Based Nonlinear Optical Dyes: Structural Modification of π-Linkers, J. Phys. Chem. C 122(7) (2018) 4009-4018.
[53] M.R.S.A. Janjua, M.U. Khan, B. Bashir, M.A. Iqbal, Y. Song, S.A.R. Naqvi, Z.A. Khan, Effect of π-conjugation spacer (C C) on the first hyperpolarizabilities of polymeric chain containing polyoxometalate cluster as a side-chain pendant: A DFT study, Comp. Theor. Chem. 994 (2012) 34-40.
[54] M.R.S.A. Janjua, M. Amin, M. Ali, B. Bashir, M.U. Khan, M.A. Iqbal, W. Guan, L. Yan, Z.M. Su, A DFT Study on The Two-Dimensional Second-Order Nonlinear Optical (NLO) Response of Terpyridine-Substituted Hexamolybdates: Physical Insight on 2D Inorganic–Organic Hybrid Functional Materials, Eur. J. Inorg. Chem. 2012(4) (2012) 705-711.
[55] M.U. Khan, M. Ibrahim, M. Khalid, M.S. Qureshi, T. Gulzar, K.M. Zia, A.A. Al-Saadi, M.R.S.A. Janjua, First theoretical probe for efficient enhancement of nonlinear optical properties of quinacridone based compounds through various modifications, Chem. Phys. Lett. 715 (2019) 222-230.
[56] M.U. Khan, M. Ibrahim, M. Khalid, A.A.C. Braga, S. Ahmed, A. Sultan, Prediction of Second-Order Nonlinear Optical Properties of D–p–A Compounds Containing Novel Fluorene Derivatives: A Promising Route to Giant Hyperpolarizabilities, J. Cluster Sci. 30(2) (2019) 415–430.

[57] M.U. Khan, M. Ibrahim, M. Khalid, S. Jamil, A.A. Al-Saadi, M.R.S.A. Janjua, Quantum Chemical Designing of Indolo [3, 2, 1-jk] carbazole-based Dyes for Highly Efficient Nonlinear Optical Properties, Chem. Phys. Lett. 719 (2019) 59-66.
[58] P.N. Prasad, D.J. Williams, Introduction to nonlinear optical effects in molecules and polymers, Wiley New York1991.

Credit Author Statement

Dear Editor,

Spectrochimica Acta Part A: Molecular and Biomolecular Spectroscopy

Authors Name	Contribution
Abdul Rauf Raza	Conceptualization, Project administration, Methodology, Supervision, Writing - review & editing
Bushra Nisar	Formal analysis, Investigation, Writing - review & editing
Muhammad Khalid	Conceptualization, Project administration, Software, Formal analysis, Supervision, Writing - review & editing
Humaira Yasmeen Gondal	Formal analysis, Investigation, Data curation
Muhammad Usman Khan	Writing - review & editing, Data curation, Investigation, Formal analysis
Sara Figueirêdo de Alcântara Morais	Resources, Data curation, Formal analysis, Writing
Muhammad Nawaz Tahir	Formal analysis, Investigation, Methodology, Writing
Ataualpa Albert Carmo Braga	Funding acquisition, Software, Resources, Review & editing

Warm Regards

Most sincerely,

Dr. Muhammad Khalid (Corresponding Author**)**
Assistant Professor,
Department of Chemistry, Khwaja Fareed University of Engineering & Information Technology, Rahim Yar Khan-64200, Pakistan
Email: khalid@iq.usp.br ; muhammad.khalid@kfueit.edu.pk

Declaration of interest

Dear Editor,

Spectrochimica Acta Part A: Molecular and Biomolecular Spectroscopy

All the co-authors are aware of and approve of the submission.

Conflict of interest

No conflicts declared.

Warm Regards

Most sincerely,

Dr. Muhammad Khalid (Corresponding Author**)**
Assistant Professor,
Department of Chemistry, Khwaja Fareed University of Engineering & Information Technology, Rahim Yar Khan-64200, Pakistan
Email: khalid@iq.usp.br ; muhammad.khalid@kfueit.edu.pk

Graphical abstract

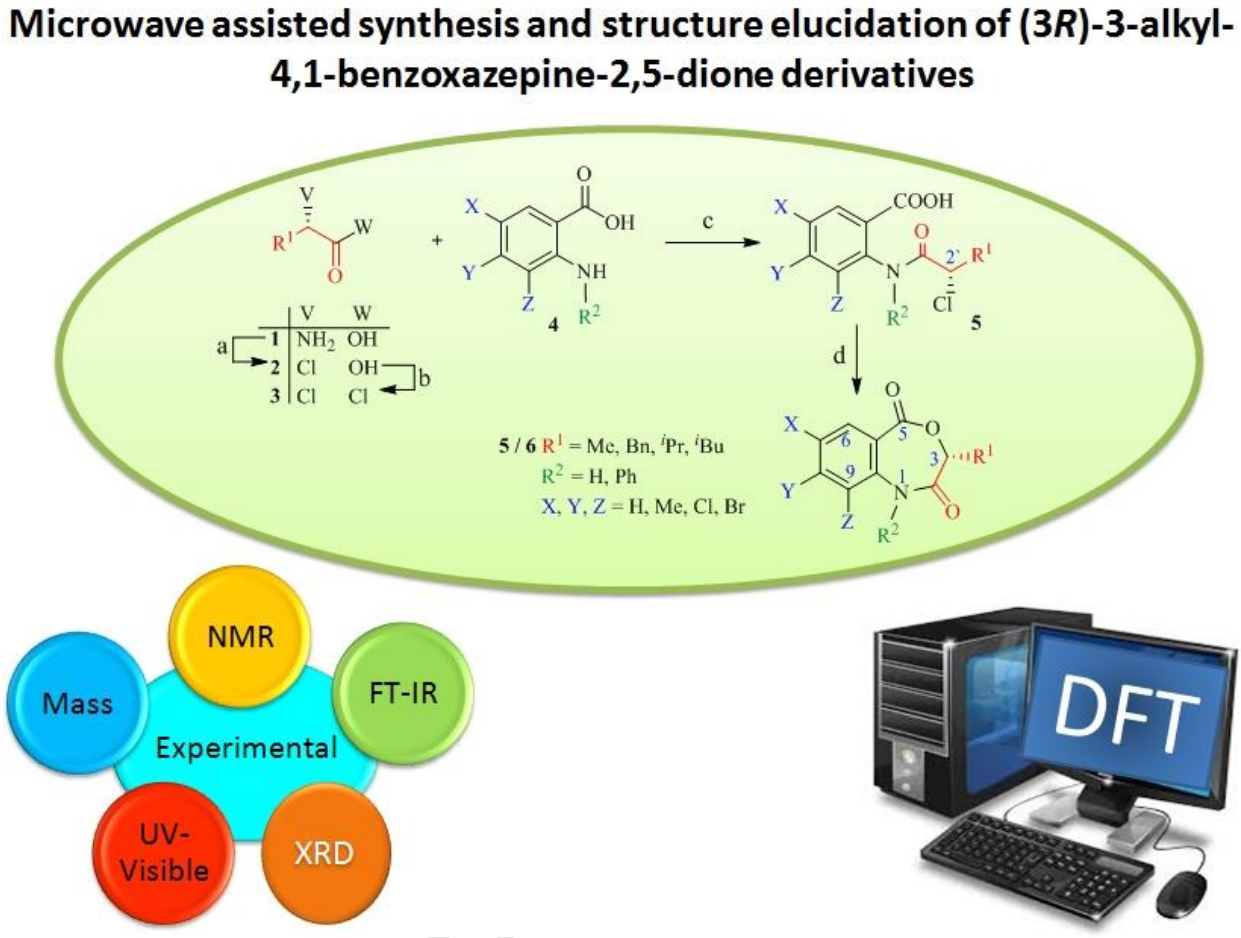

Highlights

- Four novel (3*R*)-3-alkyl-4,1-benzoxazepine-2,5-dione derivatives were synthesized by facile microwave assisted synthesis.
- SC-XRD, ^{1}H-NMR, ^{13}C-NMR, FT-IR and UV-Vis were performed for the characterization.
- Computational study was done at B3LYP/6-311+G(d,p) level for comparative analysis.
- Comparative study reveals a good agreement between experimental and DFT results.
- FMOs, NBO analysis and nonlinear optical (NLO) properties were calculated.